Development of a Hardware-in-the-Loop (HIL) Platform for Implementation of Advance Metering Functions in Microgrids

By

Sergio Ivan Alzate Drada

A thesis submitted in partial fulfillment of the requirements for the degree of

MASTER OF SCIENCE

in

ELECTRICAL ENGINEERING

UNIVERSITY OF PUERTO RICO

MAYAGÜEZ CAMPUS

2018

Approved by:

Fabio Andrade Rengifo, PhD. Chair, Graduate Committee	Date
Efrain O'Neill Carrillo, PhD. Member, Graduate Committee	Date
Rogelio Palomera, PhD. Member, Graduate Committee	Date
Omar Colon, PhD. Graduate Studies Representative	Date
José Colom, PhD. Department Chairperson	Date

Abstract of Thesis Presented to the Graduate School
of the University of Puerto Rico in Partial Fulfillment of the
Requirements for the Degree of Master of Science

Development of a Hardware-in-the-Loop Platform for Implementation of Advance Metering Functions in Microgrids

By
Sergio Ivan Alzate Drada
2018

Chair: Dr. Fabio Andrade Rengifo
Department: Electrical and Computer Engineering Department

Distributed Generation including renewable energies have spurred the development of Microgrids as a new alternative to electric energy system. Through Sustainability Energy Center (SEC) at the University of Puerto Rico Mayagüez (UPRM) a Hardware-in-the-Loop (HIL) platform has built, this platform allows researchers, graduate and under graduate students, and others to acquire a deeper understanding of microgrids, microgrid integration and control, and renewable energy. This thesis presents the design and implementation of the flexible and modular HIL platform focusing in energy management system (EMS) and advance metering applications. Experimental results of an EMS with configured demand response programs using meter data in a scenario with software modeled and hardware under test components is developed and presented.

Resumen de tesis presentado a la Escuela Graduada
de la Universidad de Puerto Rico como requisito parcial de los
requerimientos para el grado de Maestría en Ciencias

Desarrollo de una Plataforma de Hardware-in-the-Loop para la Implementación de Funciones de Medición Avanzada en Microrredes

Por
Sergio Ivan Alzate Drada
2018

Consejero: Dr. Fabio Andrade Rengifo
Departamento: Ingeniería Eléctrica y Computadoras

La generación distribuida incluyendo el uso de energías renovables han estimulado el desarrollo de las microrredes como un nuevo paradigma de los sistemas de energía. Por medio del Centro de Energía Sostenible (SEC) de la Universidad de Puerto Rico en Mayagüez (UPRM) se ha diseñado y construido una plataforma de Hardware-in-the-Loop (HIL) que permite a los investigadores, estudiantes graduados y subgraduados, así como al resto de la comunidad adquirir un conocimiento profundo de las microrredes y energías renovables, su integración y control. Este trabajo presenta el diseño e implementación de una plataforma de HIL modular y flexible enfocada en aplicaciones de sistemas de manejo de energía (EMS) y medición avanzada de energía. Se desarrollan y presentan resultados experimentales de un EMS con programas de respuesta de demanda configurados usando datos de medidores inteligente en un escenario con componentes modelados por software y componentes como hardware bajo prueba.

To my wife.

Acknowledgements

The author recognizes partial support from the National Science Foundation (NSF) under award number ACI – 1541106.

The author recognizes partial support from the Center for Grid Engineering Education (grided.epri.com) under the US Department of Energy award number DE-EE0006338.

The author recognizes support from Texas Instruments that donated the meters installed in the platform and other devices that will allow to integrate the meters in the platform by communication.

The author recognizes support from Sustainable Energy Center (SEC) research team that was part of the physical design and construction of the Hardware-in-the-Loop platform.

Contents

List of Tables

List of Figures

Chapter 1

INTRODUCTION

Alongside with current technological advances, energy consumption is becoming increasingly large. World's electricity systems, with its traditional energy models, have been questioned because they are based mainly on fossil fuels (oil, coal, natural gas). Nowadays, environmental and sustainable development needs are increasingly demanding an energetic paradigm change.

The incorporation of different types of renewable energy generators have shown a new path for electrical systems' orientation. In order to offer a service with more autonomy, the microgrids appear. There are new structures of low scaled electric grid with some independence.

This change of paradigm includes the integration of the traditional grid, distributed generation, energy renewables penetration, and microgrids, all of it in a new concept known as smart grid. Nowadays, this platform has big challenges that are the focus of current investigations as advance control systems, data administration, renewable penetration, grid stability, advance metering systems, grid resilience, energy optimization, energy consumption behaviors, energy market structures, network and communication systems, storage technologies, etc.

Considering the fact that Puerto Rico has a large annual solar energy [1] and in general, an abundant availability of renewable energy resources, it is mandatory to eliminate the dependency on fossil fuels. Consequently, a large penetration of renewable energy into the electricity grid is expected. According to Puerto Rico's public Law 82 of 2010 [2], it demands from the Puerto Rico Electric Public Authority (PREPA) to increase to 15% the renewable energy production by year 2020. Current statistics shows that Puerto Rico had a 2.1% of renewable energy production in 2016 [3], showing that the efforts made are not enough.

The investigations oriented to offer technical solutions to the current challenges require efficient design and testing methods with a high level of flexibility and adaptability to a different scenarios. To encourage the implementation of distributed generation systems using renewable energy sources and its integration with the new structures of smart grids, the Sustainability Energy Center (SEC) in the University of Puerto Rico at Mayagüez (UPRM) had the need to develop a Hardware-in-the-Loop (HIL) platform that enables research in advanced topics and supports the integration and penetration of renewable energy in a larger scale. With the implementation of this project, the SEC would have the capacity of training students, professionals and communities in basic and complex topics related to microgrids, smart grids, distributed generation, and advanced control performing scenarios without having all the hardware components [4][5].

According to [6][7], Hardware-in-the-Loop (HIL) is a methodology increasingly recognized as an effective approach for simplifying the design and testing of hardware systems in a lot of research sectors. This is because traditional software-based simulations do not have the performance required to replicate real-time operational conditions.

The purpose of this work is to develop a platform that allows the user to design and develop different advance metering scenarios in a microgrid setup, with the flexibility and modularity to use different type of components, to evaluate and test the performance without having all the real components, complete environment or particular variable behaviors. The testing application to develop in this work is an EMS with Demand Response (DR) capabilities that allows a desired balance between power generation and consumption.

Chapter 2

OBJECTIVES

This section describes the objectives that have been formulated for the proposed work. First, the general objective is presented and then the specific objectives.

2.1. General Objective

The main objective of this thesis is to develop a platform that allows the user to design and develop different advance metering applications in a microgrid scenario. The proposed platform will have a modular structure to easily modify the scenario configurations and components to create more experiments. Finally, this platform could be integrated with another platforms and power devices at the Sustainable Energy Center in UPRM.

2.2. Specific Objectives

2.2.1. To identify the smart grid infrastructure and most used types of demand response programs.

2.2.2. To develop a real-time HIL platform for perform advance metering applications.

2.2.3. To validate a Microgrid scenario with demand response function in the real-time HIL platform.

Chapter 3

LITERATURE REVIEW

In this chapter, the background needed to design and implement a platform with real Smart Grid structure and with current advance metering capabilities.

3.1. Background

In this section, the definition of smart grids and its components are described. Also, a review of Hardware-in-the-Loop (HIL), demand response, a list of demand response programs and a review of advanced metering infrastructure are shown.

3.1.5.1. Hardware-in-the-Loop (HIL)

Traditional methods to perform systems include performance tests of the entire system in software simulations or experimentation on real hardware. HIL appears with the need of efficient testing methods when the testing scenario has limitations (economical or physical) and require more flexibility than the traditional testing methods [8].

The combination of a system simulation with hardware experimentation is known as HIL. When the hardware include power components, there is a distinction between power HIL and control HIL[8]. In HIL systems, a simulation in real time runs in a dedicated hardware. The simulation interacts with the device under test. The response' feedback from the device works as an electrical signal which closes the loop and generates a complete simulated machine/environment[9]. Figure 1 shows a graphic representation of power HIL testing method.

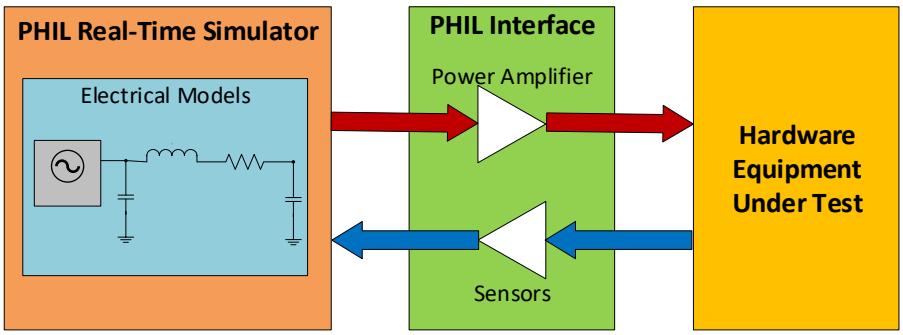

Figure 1. Concept of power Hardware-in-the-Loop testing method (figure adapted from [10]*)*

One of the benefits of the use of HIL in testing is that particular hardware could be used in combination with a software simulation of the rest of components, instead of use complex software models that only represents an approximation of the real behavior. According to this, the accuracy of the results in traditional software methods depends on the approximation of software modelling and the computing power of the machine where the software runs[8].

Another significant benefit is that HIL offers a great modularity and flexibility platform when designing and performing test scenarios. It allows to do modifications on components without impact the infrastructure, operation or functionality of the other components or the complete system.

3.1.5.2. Smart Grids

According to the Department of Energy of United States, the Smart Grids are a response to the necessities to improve the traditional grid in order to integrate all the emerging energy structures, as well as to make the current grid smarter and more resilient using cutting-edge technologies, equipment, and controls, working together to deliver electricity more reliable and resilient to external impacts [11].

In a report published by the National Institute of Standards and Technology (NIST) [12], a framework and roadmap for Smart Grid interoperability standards are presented. The document includes a conceptual domain model that describes the main domains that specifies the Smart Grid conceptual roles and services. The domains described in the report are: customer, markets, service provider, operations, generation, transmission,

and distribution. Next, as an adaptation of the framework presented by NIST, there is a description of the main elements of the smart grid infrastructure [13]:

3.1.2.1. Remote Terminal Units (RTU)

Are terminals that allow remote monitoring and controlling of different places of the process as power generators and some actuators. The RTU get field measurements to serve data to the SCADA in real time [13]. Conventional SCADA systems are based on RTU devices, but due to its asynchronous nature and relative slow rates, these devices do not accurate angle difference information from two buses in the power network. To provide real-time phase angles with higher accuracy, Phasor Measurement Units are used in current implementations [14].

3.1.2.2. Supervisory Control and Data Acquisition (SCADA)

Component that collects data from RTU measurements located in different places of the network. Through the SCADA, the main variables of the process are monitored, and operation decisions about the system's behavior to control the whole operation are taken. Some of the variables monitored by the SCADA are weather conditions, power production, equipment status, grid conditions, miscellaneous electrical measurements, operation status variables, etc. An important feature of the SCADA is to operate the active and reactive generation of bulk and distributed generators depending on the needs of the loads [13].

3.1.2.3. Energy Management System (EMS)

Used to monitoring, controlling, and to get an optimum performance of the system and operation in the Smart Grid infrastructure. The EMS run with data collected by the SCADA that supports the decision making for the optimization of the Grid [13]. The decision making in an EMS is also supported by load forecasting, weather and power prediction, and electricity markets information. It is also used to lead savings in the overall operating costs [15].

Due to the variety of Distributed Energy Resources (DER) that are included in the Smart Grids and microgrids operation, mechanisms such as Distributed Energy Resources Management Systems (DERMS) are included in the structure. DERMS provides the system with capabilities to optimize the management and control of the demand-side programs and the DERs to accomplish economic and reliability objectives for the grid operation [16]. DERMS collects the data measured by sensors through communication networks and classifies situational activities of energy consumption [17].

3.1.2.4. Advanced Metering Infrastructure (AMI)

Smart metering system that is in the ability to have a bidirectional communication with other components of the system [13]. Main functions of the AMI include the measurement, collection, transference, and analysis of energy usage. This system enables the users to participate in programs to reduce peak demands and in contribute to energy management process [18]. This system is based in a robust communication infrastructure with universally acceptable standards. Design of this network architecture is focused on get low throughput data network due to the high quantity of communication components [19].

3.1.2.5. State Estimation Algorithms (SEA)

Set of mathematical methods and procedures used to evaluate the state of the Grid using the data measured in RTU. It is used to make the entire control of the grid and to capture the information in real time [13]. This type of systems are necessary due to the big quantity of measurements and locations in a power grid [20][21].

3.1.2.6. Power Generation and Load Forecast System (GLFS)

The utilities have as an objective to balance the power generation and the demand, with the aim to offer a good and competitive service. This system realizes the predictive analysis from the information allocated in the SCADA [13]. Due to the increasing amount of renewable energy integration the accuracy of the forecast methods affects directly to the system stability and economic operation[22].

Figure 2 shows a graphical representation of the infrastructure described above.

Figure 2. Smart Grid infrastructure (Adapted from [13])

3.1.5.3. Microgrid

Microgrids are low voltage distribution grids (sometimes medium voltage) mainly composed by one or more distributed generators (DG), storage systems and controlled loads. Microgrids could operate in islanding mode or grid connected and synchronized with the utility grid [23].

Some of the benefits that generates the microgrids are: support in increase of renewable penetration, gas emission and fossil fuels generation dependency reduction, indirect losses reduction of traditional transmission and distribution grid structure, autonomous operation when utility grid goes to a blackout [24][25].

An adaptation of ISA-95 (Enterprise-Control System Integration Standard) developed in [26], describes the Microgrid hierarchical control levels.

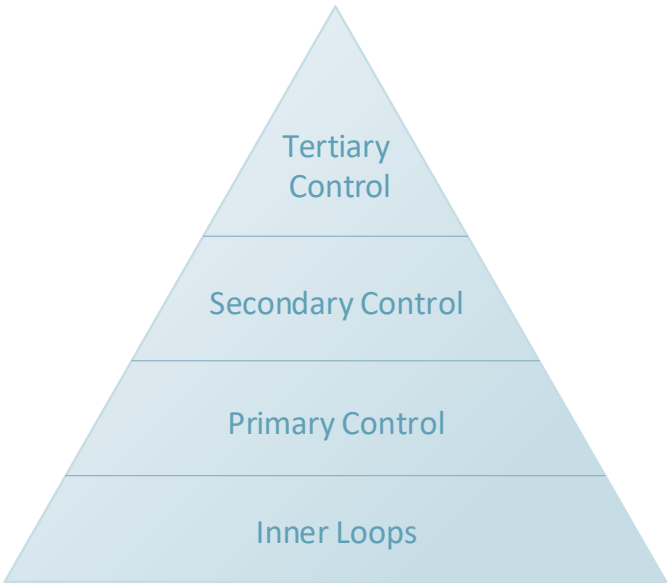

Figure 3. Microgrid hierarchical control levels

- Level 3 (tertiary control): power flow control between the Microgrid and the grid, energy market.
- Level 2 (secondary control): synchronization control loop, connection and disconnection from distribution system, power quality.
- Level 1 (primary control): active and reactive power droop-control.
- Level 0 (inner control loops): regulation control loops. Voltage and current, feedback and feedforward, linear and non-linear control loops.

3.1.5.4. Advance Metering

According to FERC, advance metering are systems which captures and records customer energy consumption behavior in a defined period, and transmits the information obtained through a communication network to a central collection point [27].

A Smart Meter is an advance energy meter that obtains electric information from every measurement point and provides the information to a utility company and/or system operator mainly for monitoring and billing. This information is measured in real time and logged in specific structures. Bidirectional communication and load control are the main feature of a smart meter [28].

A typical AMI infrastructure components are presented in [29] specifies the information flow in a AMI application, graphically represented in Figure 4. The electrical measurements are registered by a smart meter located in a house in a HAN (Home Area Network). The information collected by the smart meters is transmitted to a data concentrator by a NAN (Neighborhood Area Network). The data concentrator process data from several smart meters and this information is transmitted to a Head-end-System (HES) through an WAN (Wide Area Network). From the HES, the information is distributed to the different systems in the Smart Grid infrastructure by a Meter Data Management System (MDMS). All the described communication systems are bi-directional.

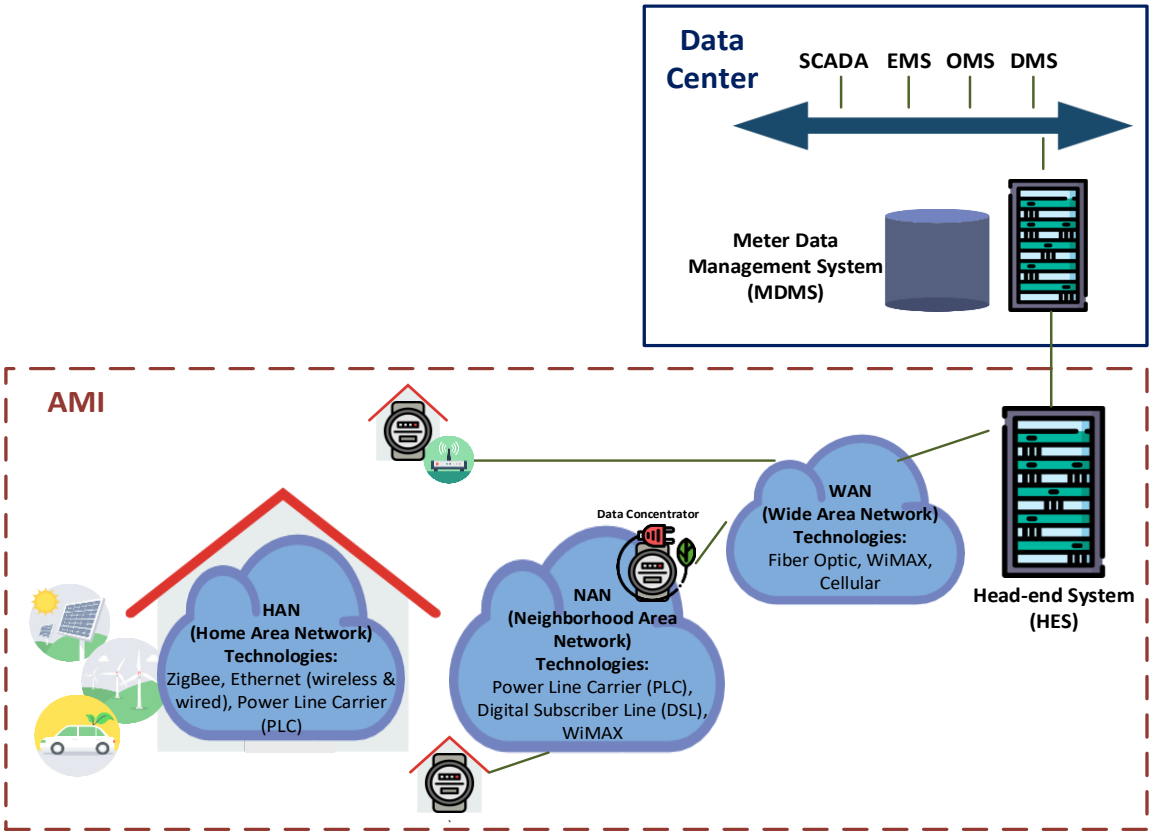

Figure 4. Typical AMI infrastructure (adapted from [29])

3.1.5.5. Demand Response (DR)

According to FERC (Federal Energy Regulatory Commission), Demand Response (DR) is a change of normal patterns of energy consumption in customers in response of a specific tariff or incentive program designed to reduce usage of electricity when grid

reliability is jeopardized [27]. One of the main goals of DR is to get a balance between generation and consumption.

The active participation of end-consumers is a very important factor in DR, and is a direct reaction of incentive pricing, new tariff schemes, education, and feedback, implemented by the policies [30].

There are two groups of DR programs: incentive-based DR and time-based rates DR. A list of different types of programs are stated below [31]:

3.1.5.1. Incentive-Based DR:

- Direct load control (DLC): utility or grid operator gets free access to customer processes.
- Interruptible/curtailable rates: customers get special contract with limited sheds.
- Emergency demand response programs: voluntary response to emergency signals.
- Capacity market programs: customers guarantee to pitch in when the grid is in need.
- Demand bidding programs: customers can bid for curtailing at attractive prices

3.1.5.2. Time-Based Rates DR:

- Time-of-use rates: scheduled fixed price blocks.
- Critical peak pricing: pre-specified rates triggered by the utility for a limited time.
- Real-time pricing (RTP): continuous variation of rates in response to wholesale market prices [32].

3.2. Previous Related Studies

In this section are presented some similar investigations that are used as base knowledge to define a research framework. Each investigation referenced is synthesized and analyzed according to its similarities and differences to our research frame.

There are several works that are focused in a HIL platform development for power electronics devices testing. The work described in [7], is a low-cost real time HIL platform for power electronics applications testing. In this work the authors use a real time application interface (RTAI) from an open source Linux kernel modification package to

accomplish a HIL simulation and the validation of power electronics control applications as a boost converter and an H-bridge inverter. A similar work presented in [6] shows the design and development of a HIL system for simulation of electrical machines for testing power electronic products. This work shows experimental results of the components and features testing of a drive inverter. These two works are related to our work because of the implementation of a real-time HIL platform to validation of power electronics applications. However, the two works differs because of the validation scenario that we propose. It is not only power electronics, but in a complete microgrid infrastructure focused in advance metering functions.

In [33], the authors presents the design and implementation of a smart meter with demand response capabilities. They presented an advanced metering infrastructure (AMI) with an energy management system (EMS) scenario where the demand response capabilities are simulated testing a time of use (TOU) program in a traditional grid infrastructure. The platform used to develop the smart meter is a microcontroller Raspberry Pi connected by ethernet with the EMS developed in a computer. The demand response processing is executed by a knowledge based fuzzy controller (KBFC). It is related to our work because of the implementation of an EMS and advance metering functions to execute demand response programs. However, it differs in the software and hardware platform used, because they use a low-cost processing device and is not a HIL platform that runs in real-time. This work is also different in the scenario where DR is implemented, our proposed work will implement the advance metering functions in a microgrid scenario.

In [34], the authors show a review of AMI and experimental results in a pilot project of a DR based on a smart metering infrastructure with the objective to facilitate PV integration in low voltage grids. The AMI research in this work is focused in a real communication infrastructure located in Switzerland and developed by Utility of the Canton of Zurich (EKZ), Landis+Gyr and the Swiss Federal Institute of Technology (ETH) Zurich in 2011. The system developed in this work validates the DR functions using heuristic control and model predictive control, acquire PV power forecast from the

company SteadySun, and Load Power Demand forecast from several machine learning techniques on historical data. It is related to our work because of the testing scenario of the advance metering functions. However, it differs in the use of real hardware devices for development and testing instead of the HIL platform proposed in our work. Another difference is that in the referenced work, the control system is based on predictive strategies.

An central EMS of a microgrid and a local power management system at the customer side is presented in [35]. The microgrid proposed in this work is composed by a PV generators, embedded storage units and a gas microturbine. The EMS developed in this work is focused in a techno-economic optimization of power and energy management based in load forecasting, power prediction, electricity markets, and power/energy availability on distributed generators. It is related to our work because of the implementation of an EMS and the similar component structure developed in the microgrid. The difference is that our work is focused in the development of a modular and flexible HIL platform to implement different microgrid scenarios.

The work described in [36], shows the development and experiment results of a HIL real-time digital simulator (RTDS) model of an existing microgrid that communicates over Internet in real-time with a centralized microgrid power management and control system. The two real-time simulation and control facilities used in this project are located on opposite sides in United States, the microgrid model is located in Florida State University and the microgrid model is located in University of California San Diego. The paper describes the development of the microgrid components model and the control algorithms design. The developed controller has the ability to compute a power reference for the microgrid, adjust the power to that reference, and control the state of charge (SoC) of the storage unit within the microgrid simultaneously. It is related to our work because of the microgrid testing scenario and the use of a HIL platform to perform the experiments. However, it differs in the use of only microgrid modelled components, instead of real hardware on test integrations to HIL platform as proposed in our work. Another difference is that the described work uses internet communication to accomplish

the link between the microgrid and the control system, that makes the work focus on the performance of the communication channel.

A significant scope of our work is the use of microgrid component models. There are several works that are focused in electrical modeling. The work described in [37], shows a photovoltaic electrical model based on the Shockley diode equation and its use to test and compare the maximum power point depending of the temperature and irradiance. In [38], a photovoltaic array model is presented. This work describes the mathematical model based only in the panels specification parameters provided by the manufacturers datasheets and integrate the model with a Maximum Power Point Tracker (MPPT) technique.

A modular structure of wind turbine modules is presented in [39]. This paper describes generic simulation models for wind turbines and wind power plants and its interfaces with grid models. In [40], a wind turbine mathematical model is developed and simulated. This paper develops and simulate in MATLAB a wind speed, wind wheel, driving mechanism, power generator, and wind power models including the pitch control system.

The work described in [41], presents an electrical battery model based on a Thevenin circuit with two RC parallel branches considering the battery state of charge estimation and hysteresis. Another battery model is presented in [42]. the paper describes a lithium-ion battery mathematical model based on data obtained from a real battery, taking account the operating temperature and charge/discharge current rates.

The work presented in [43], shows different types and modeling tools used to model, simulate and test electric and hybrid vehicles. This journal uses experimental models based tools as Advanced Vehicle Simulator (ADVISOR), Powertrain System Analysis Toolkit (PSAT), and some physics based tools as VTB, PSIM, Simplorer, and V-Elph. This work describes, simulates, and compare the different modeling techniques with the numerical result analysis.

The component models presented in these references are useful because they are mathematical models of microgrid components that could be used to implement software modeled devices in a HIL microgrid scenario [37]-[43].

The main difference between our purpose work and the others presented before, is the development of a platform that allows the user to design and develop different application scenarios in a microgrid setup, with the flexibility to use different type of components, and to evaluate and test the performance without having all the real components, complete environment or particular variable behaviors. Modularity and flexibility are the main features of the proposed work, because it allows the user to change or add any components without impacting the infrastructure, the operation, or the functionality of other components or the complete system. The testing application to develop in this work is an EMS that allows a desired balance between power generation and consumption.

Chapter 4

CONCEPTUAL SYSTEM DESIGN

The design of the platform is focused in getting a high modular and flexible structure. It allows to change or add any components without impacting the infrastructure, the operation, the functionality of other components or the complete system. Based on the Hardware-in-the-Loop concept and benefits, the platform has the capability to execute scenarios with all the components modeled in software or scenarios with software and hardware component combinations.

According to the definition of components in a smart grid infrastructure described in Chapter 2 and keeping in mind that the objective of the platform is to develop different advance metering applications in a microgrid scenario, an inverter-based conceptual infrastructure was designed. Figure 5 shows the most basic scenario that can be implemented to perform an experiment in the proposed platform.

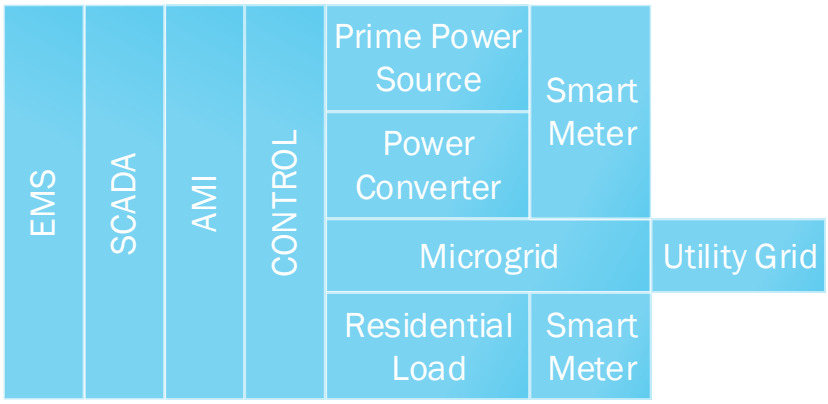

Figure 5. Basic conceptual scenario

Each functional component of the scenario has a performance that generates an output outcome depending of input parameters. Components in the experiments could be software-modeled types or real devices under test, depending of the limitations and objectives of the scenario to perform. Next, there is a characterization of each type of component in the proposed scenario.

4.1. Prime Energy Source

The behavior of the prime energy source is strongly linked to the type of energy source used. This component could be replaced by a fixed DC power source, programmable DC power source, a photovoltaic panel, a wind turbine, a battery storage, and an electrical vehicle among. The input parameters for each one could be different, but the common output is the generated DC current and voltage.

Figure 6 describes the input and output parameters that have each type of component that could be used as prime energy source in the platform.

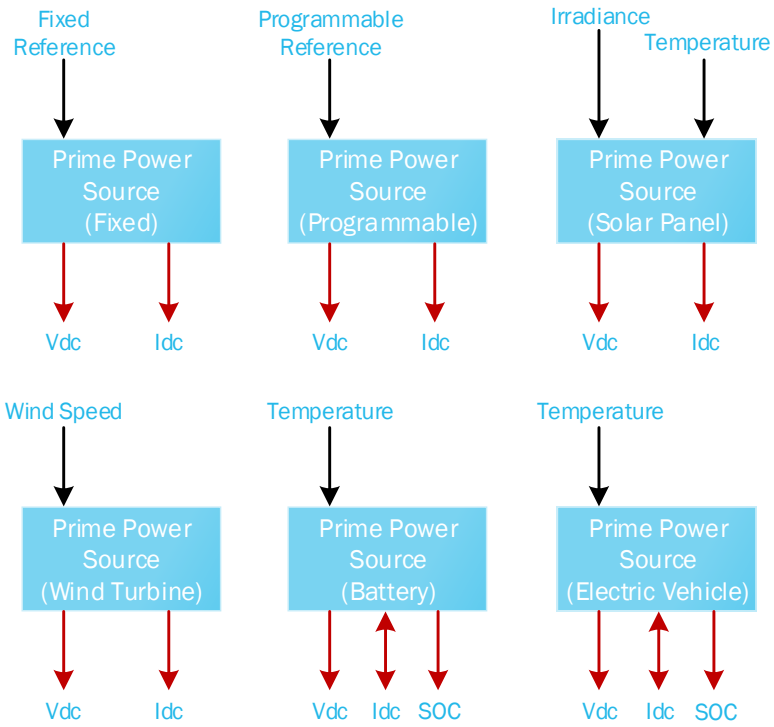

Figure 6. DC source conceptual model

4.2. Power Converter Interfaces

The main function of the power converters interfaces is the DC/AC or AC/DC energy conversion. The power flow could be unidirectional or bidirectional depending on the application and power source. The input and output parameters associated to the power converters interfaces are voltages, currents in DC and AC, and the control signals. Figure 7 shows the input and output parameters characterization of the power converter interfaces.

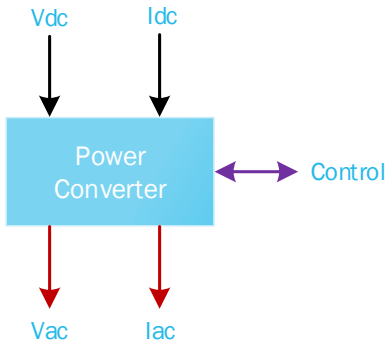

Figure 7. Power converter conceptual model

4.3. Smart Meter

The measured node delivers to the smart meter the AC voltage and current, with these values the meter process all the calculations and send via communication all the information to another component. The meter calculations include frequency detection, active and reactive power, energy consumption, total harmonic distortion and harmonic components, and average values. Figure 8 shows the input and output characterization of the smart meter component.

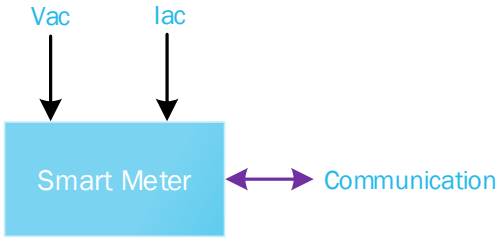

Figure 8. Smart meter conceptual model

4.4. Microgrid

The microgrid behavior depends of power distribution system configuration and the power sources and electrical loads connected to it. The inputs and outputs of the system are the voltages and currents of each component, and the power flow depends of the components type and the implemented scenario. The microgrid model could be an ideal one as a single node or a complex model with additional parameters such as voltage unbalances and another electrical problems. Figure 9 shows the conceptual characterization of the Microgrid.

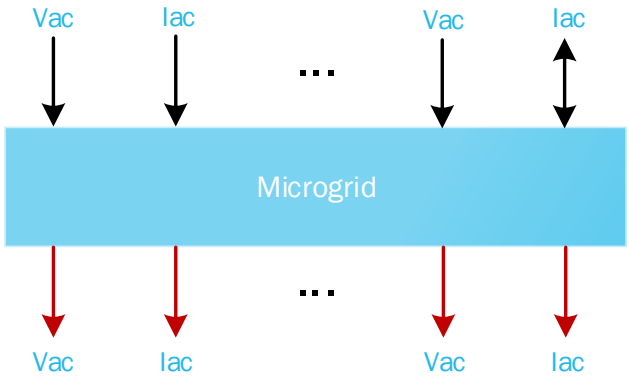

Figure 9. Microgrid conceptual model

4.5. Utility Grid

The electrical grid performance could be used as an ideal infinite power source or an entire complex system with power generation, transmission and distribution subsystems. The AC voltage is an output of the component and the AC current could be an input or output depending of the power flow in the microgrid. Figure 10 shows the utility grid conceptual characterization.

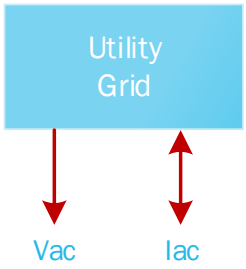

Figure 10. Utility grid conceptual model

4.6. Load

The power consumption behavior depends of the type of load used in the experiment. This component could be replaced by a fixed load, a programmable load, or a real load as shown in Figure 11. Also, this can be both linear or nonlinear loads. The load has as input the voltage and the current that depends of the consumption behavior.

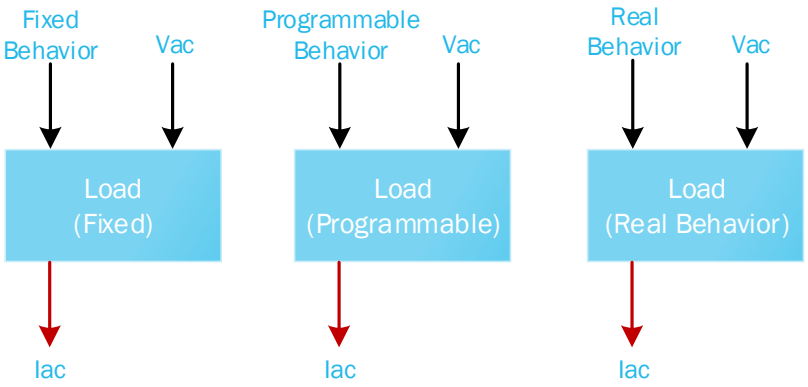

Figure 11. Residential load conceptual model

4.7. AMI

This component is composed internally by a communications network, receives by communication the data from the meters and delivers by communication the information packages to the next hierarchical smart grid level as shown in Figure 12. The AMI could be implemented as a physical infrastructure or assumed as an ideal communication bus without delays.

Figure 12. AMI conceptual model

4.8. EMS / SCADA / Control

Although the three components are physically independent, can be characterized as a parameter hub, because receives a variety of parameters, process the information and do calculations, as well as refresh the output parameters. Figure 13 shows this components conceptual model.

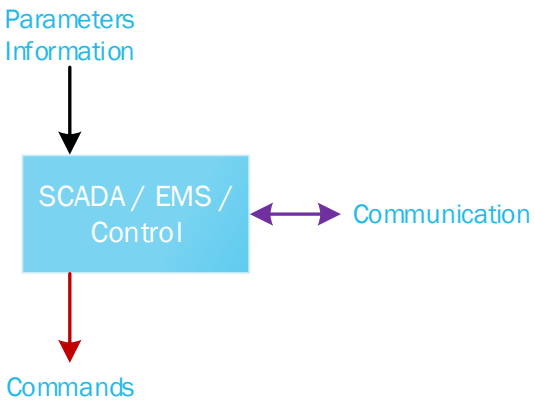

Figure 13. EMS / SCADA / Control conceptual model

Understanding the modular platform concept with the expected capabilities, the developed applications or experiments could be as complex and extensive as desired. The only limitation of the projected experiments are the physical limitations and the processing power of the HIL module. Figure 14 shows a conceptual example of the expected capabilities of the platform.

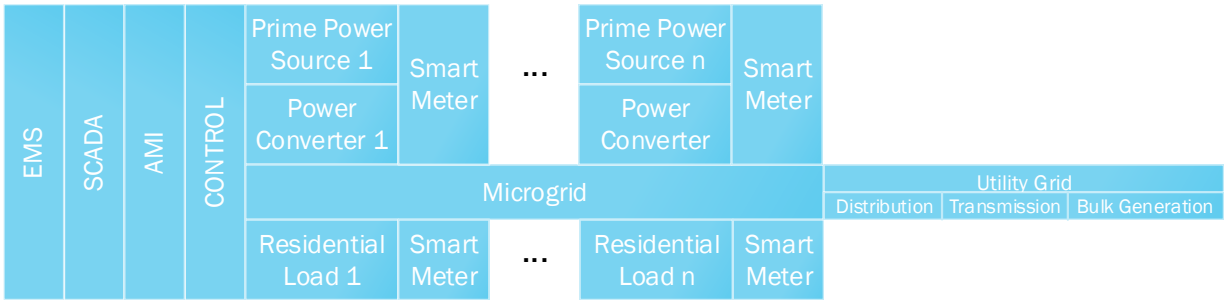

Figure 14. Platform conceptual projection

Chapter 5

PLATFORM TECHNICAL DESCRIPTION

The HIL setup is a powerful tool with a high level of flexibility and modularity to accomplish different research, developments and educational work at University of Puerto Rico and with the island society. Thus, the setup can run different types of experiments and projects related to microgrids, distributed generators, renewables, smart grids, advance metering, and advance control. The system core is a HIL modular laboratory system from dSPACE technologies that allows real-time processing and integration with the other system-functional components for fast control prototyping, testing and data acquisition applications. The system is also composed by four power inverters, each one with a filter designed to control the output voltage. Table 1 shows the technical characteristics of the main devices of the setup.

Table 1. Technical characteristics of main components

Component	***Technical Characteristics***
Processor Board dSPACE 1006	Quad-core AMD Opteron 2.8 GHz processor, 1GB DDR-2-267 SDRAM memory for the application and dynamic application data, 4x128 MB DDR-2-267 SDRAM global memory for host data exchange, serial COM port and I/O module interfaces
Expansion Box – PX10	Chassis with availability to 10 full-size 16-bit ISA slots, 1 slot reserved for Link Board or slot CPU board for Ethernet connection
Analog Input Module – DS2004	16 channels for digitizing analog input signals at high sample rates, 16-bit resolution and 800ns conversion time
Digital I/O Module – DS4003	3 ports, each one with the availability of 32 I/O lines by port, each channel support TTL levels and every port needs a power supply of 5Vdc
PWM Module – DS5101_2	TTL pulse patterns on up to 16 optical channels with high accuracy, and time resolution of 25ns
Inverter – Danfoss VLT-302	2.2kW, three phases, supports a DC level input up to 400Vdc, AC output up to 690Vac, frequency output between 0 and 590Hz, PWM and digital I/O for control

The modularity of the system allows to change any component without impacting the infrastructure, operation or functionality of other components or the complete system.

The entire setup was designed to allow the connection of different types of sources, inverters, filters and loads. In addition, the multiplug at the output of each filter allows the user to easily plug modules or devices needed for each application or experiment. Figure 15 shows a general functional diagram of main components of the setup. The descriptions of the components function are listed below.

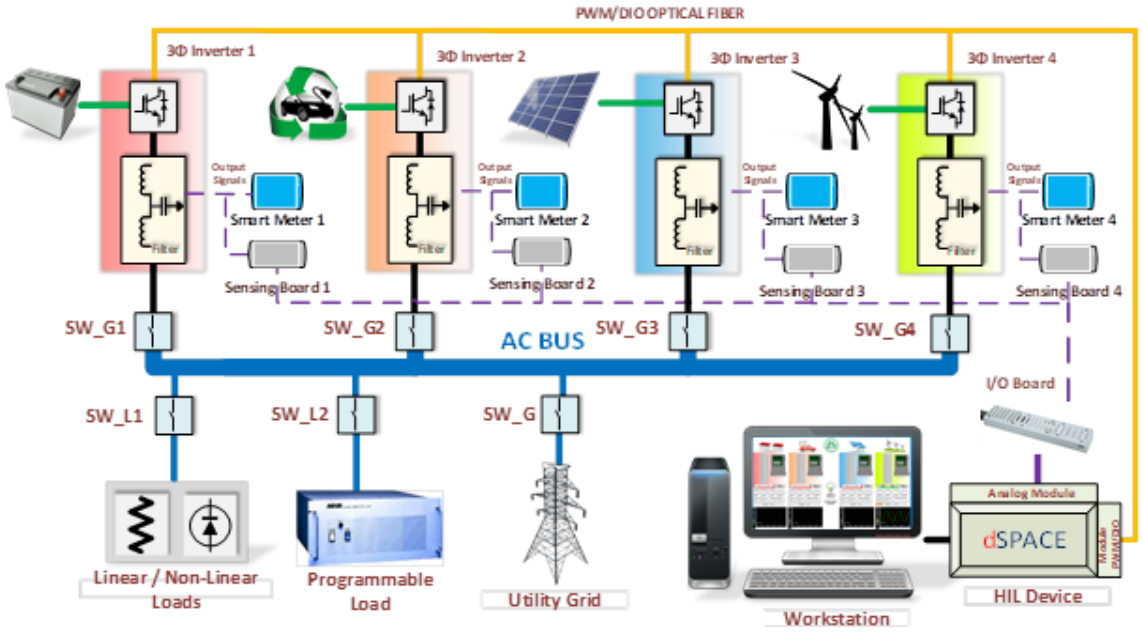

Figure 15. Platform functional diagram

Figure 16 represents the physical platform located in the Sustainable Energy Center (SEC).

Figure 16. Physical Platform Construction

5.1. HIL Modular Device

This unit is a computer system that operates with dedicated functions for real-time controlling of the system components. Complete HIL process is executed in this system. This device performs data acquisition, real-time processing and control, actuators commanding, and communication to software interface. The applications could be programmed from MATLAB Simulink via Real-Time Interface (RTI), and easily linked and deployed to the processor board with dSPACE ControlDesk application. The system is composed by the modules below:

- 1 – CPU board (ACE1006)
- 1 – Expansion box (PX10)
- 2 – 16-channel A/D boards (DS2004)
- 2 – Digital I/O boards (DS4003)
- 1 – PWM output board (DS5101)

5.2. Workstation

It is a desktop computer where the dSPACE ControlDesk runs. This application is a modular experiment and instrumentation software for electronic control unit (ECU) development. This software can be used for rapid control prototyping, hardware-in-the-loop simulations, ECU measurement, calibration, and diagnostics. In general terms, this tool deploys the customized applications and graphical interface to operate the system. Another feature of ControlDesk is the possibility to develop in Python additional functions and integrations with external applications for Real-Time testing.

The workstation is connected to the dSPACE via optics fiber. This connection is used to deploy the constructed applications through the .sdf file from MATLAB to the dSPACE and to read the variables from dSPACE to the software dSPACE ControlDesk.

5.3. Voltage Sources

It refers to the different technologies of DC voltage sources that could be used in the system. The setup has the capability to use fixed voltage sources, programmable DC voltage sources, or real energy sources such as solar panels, wind turbines, and batteries. Programmable DC voltage sources play an important role in HIL testing because the user have the possibility to generate voltage emulating desired behaviors and patterns of weather conditions in the experiments.

5.4. Power Converters

These devices together with the voltage power sources and the filter modules, are the distributed generators subsystem of the microgrid setup. It is a Danfoss Drive reconfigured with a different control board to operate as a 2.2 kW inverter. It can be configured as a DC-AC or AC-DC converter. That is, it can be configurable to bidirectional power flow applications.

An Interface and Protection board (IPC3) is internally connected to the converter inputs with the objective to provide external control over the IGBT gate drivers of the converter. This card is also used as protection against short-circuit and over-current at the output, DC over voltage, inverter-leg shoot-through, over-frequency and over-

temperature. All Logic functions are implemented on a Complex Programmable Logix Device (CPLD).

The power converters are controlled by PWM and digital signals, which are physically connected to the HIL device by optical fiber. PWM signals govern the IGBT gate drivers of each phase of the converter, and digital signals reads the status bit and controls the enable and reset commands of the converter. PWM board in HIL device have an optical fiber interface board. Using optical fiber to link the control signals it is possible to avoid electromagnetic noise due to the IGBTs of the DC/AC converters switching.

5.5. Filter Device

It is a filter module that has the main function of mitigate all the harmonics generated by the switching in the inverter and leave only the fundamental frequency signal. The filters are connected at the output of the inverters and can be exchanged depending on the experiment scenario. For example, an inductive filter could be used if a solar cell is connected to the converter, or a LC/LCL filter could be needed if the system uses a battery stack as a component of the system.

5.6. Relays

A 3-phase solid state relay is located between the output of each modular filter and the AC link to connect each inverter when the control determine that the AC generated signal is synchronized with the reference. Each relay is controlled by HIL device by a digital signal. The AC Bus can be connected to the utility grid to emulate grid-connected mode on the microgrid or be disconnected to emulate islanded-mode.

5.7. Sensor Board

The setup has the capability to integrate several types of sensors such as temperature, humidity, voltage, current, etc., needed for a particular application. It is necessary to use boards for electric signal processing and get voltage and current desired levels in the I/O modules. To acquire electrical variables of the system, a sensor board was designed and constructed. It has the function to measure the variables of the setup through the sensors LA25-NP for currents and LV25-P for voltages and deliver the signal to the HIL device analog I/O modules.

5.8. Smart Meters

Four smart meters are located in the output of each converter. They show the electrical measurements on an LCD display. The meter reference is EVM-MSP430F47197 from Texas Instruments. They have a serial communication port to integrate the devices and externally read measured and calculated variables. Integration of these devices with the HIL device is under development in an Advance Metering Infrastructure (AMI) external project.

5.9. Loads

There are several load types that are available in the laboratory and can be used in the setup applications. Depending on the experiment or application needs, the loads used could be linear, non-linear, or programmable loads. Programmable loads allow a better approximation to real scenarios in the experiments. Real loads behavior and patterns can be emulated by the device to perform measurements and results near to reality.

Chapter 6

SCENARIO DEVELOPMENT

This section describes the components, models, and structure used to develop the scenario in the platform. The scenario for this experiment is a grid-connected microgrid composed by a photovoltaic (PV) generator, an energy storage system (ESS), and three residential houses. In this case, it represents a small community. Taking for granted the functionality of the lower operational control levels of the microgrid that allow the power regulation, power generation, and power sharing in the microgrid, the experiment is focused in an Energy Manage System (EMS) that operates based in the power generation of the grid, the PV system generation, battery power, loads consumption, and state of charge (SOC) of the batteries.

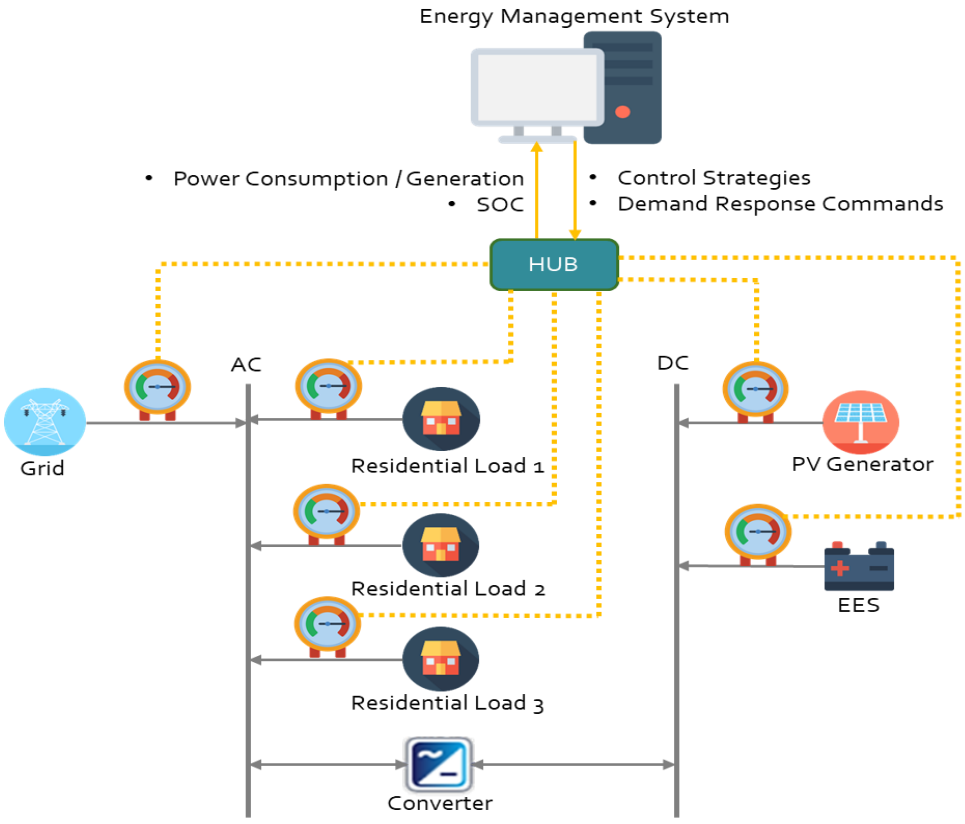

Figure 17. Developed scenario functional diagram

The objective of the EMS is to maximize the PV generation and to maintain a constant flow from the electrical grid, preserving the stability of the grid keeping a flat power demand. Input parameters of the control in the EMS are collected through smart meters located in each component of the microgrid. Figure 17 shows the component functional diagram in the described scenario.

Next, the development and model details of each component of the scenario are described:

6.1. SCADA

This component was developed in the software dSPACE ControlDesk located in the setup workstation. The SCADA application includes the user graphic interface through the custom displays developed to show the main parameters, variable trends, and operation of each scenario component. The application also has the capability to save a record of the measured variables to a better data analysis of the simulations. The SCADA hierarchical structure application is presented in Figure 18.

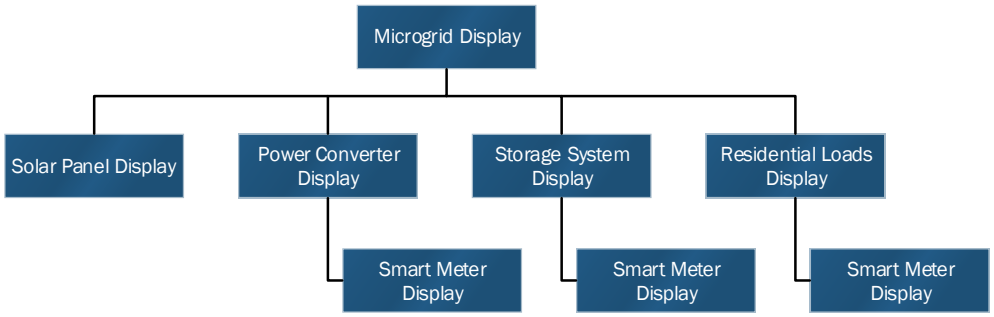

Figure 18. SCADA hierarchical structure

The main scenario display is shown in Figure 19. It includes the whole vision of the microgrid, system components, main electrical parameters, and a tracking behavior of the variables. At the left side of the display, the single line diagram with the value of the main electrical parameters of each component of the system are shown. At the right side, the graphical trends that represent the behavior of the main variables of the system are shown.

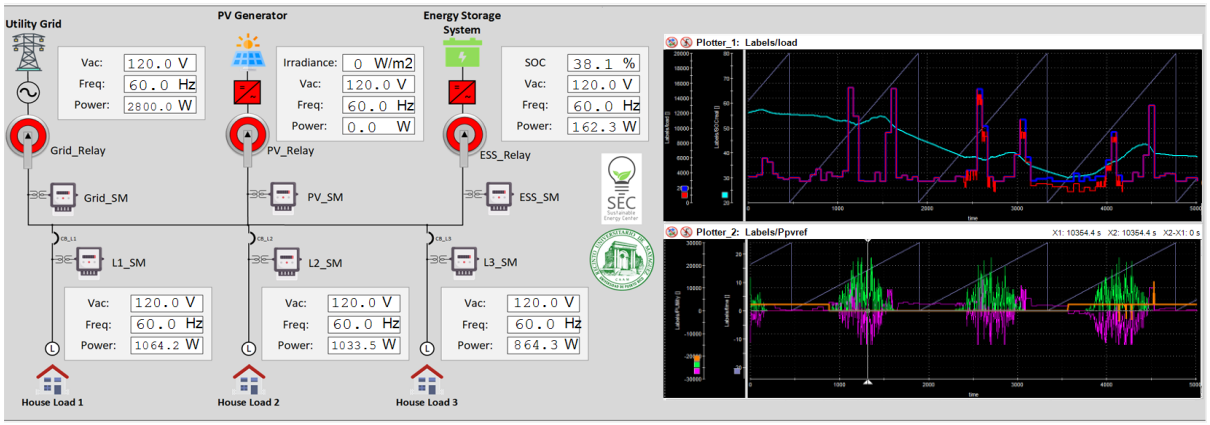

Figure 19. SCADA Microgrid main display

The other displays of the SCADA structure will be described in each scenario component section.

6.2. Solar Panel

A 25 kW photovoltaic panel model was developed with the objective to simulate a real behavior of solar energy production. The model used in the experiment is proposed in [37], it is based on the Shockley diode equation. The behavior of the solar cell is modelled as a photo-current source, a single diode junction and a series resistance as presented in Figure 20. This model evaluates the electrical DC output from solar irradiance and temperature parameters.

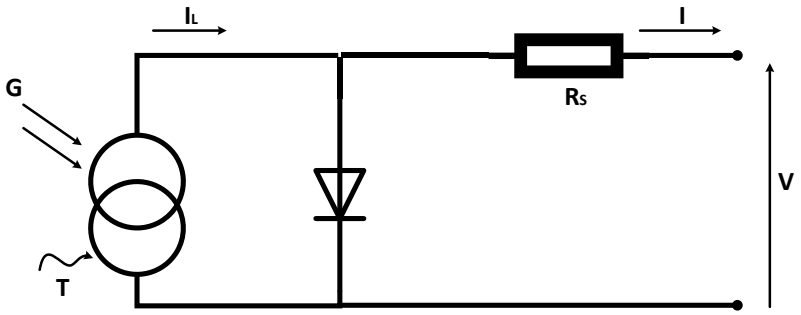

Figure 20. Circuit diagram of PV model (adapted from [37])

The equations that describe the behavior of the voltage and current presented in [37] are detailed in Appendix A.

To get the closest solar panel real behavior, all the constant parameters in the equation was replaced using the manufacturers ratings of a commercial photovoltaic

panel. The selected panel to be used in the scenario is the Solarex MSX60 60W. The main typical electrical parameters of the photovoltaic module obtained in the product data sheet and in [37] are listed below:

Table 2. Typical electrical parameters of Solarex MSX60 60W

Parameter	Description	Value	Unit
k	Boltzman's Constant	1.38E-23	J/K
q	Charge on an electron	1.60E-19	C
Rs	Series resistant	8	mΩ
Rp	Parallel resistant	200	Ω
n	Diode quality factor	1.2	
Isc	Short circuit current	3.8	A
Voc	Open circuit voltage	21.06	V
Vg	Band gap voltage	1.12	eV
Vm	Voltage, maximum power	17.1	V
Im	Current, maximum power	3.5	A
Pm	Maximum power	59	W

The behavior of the photovoltaic model was validated with a comparison between the panel voltage and current characteristic curves obtained by the MATLAB code (see Figure 21) with the curves presented by the manufacturer in the product data sheet and the results presented in [37]. The characteristic curves were obtained with standard test conditions (STC) using one solar panel cell.

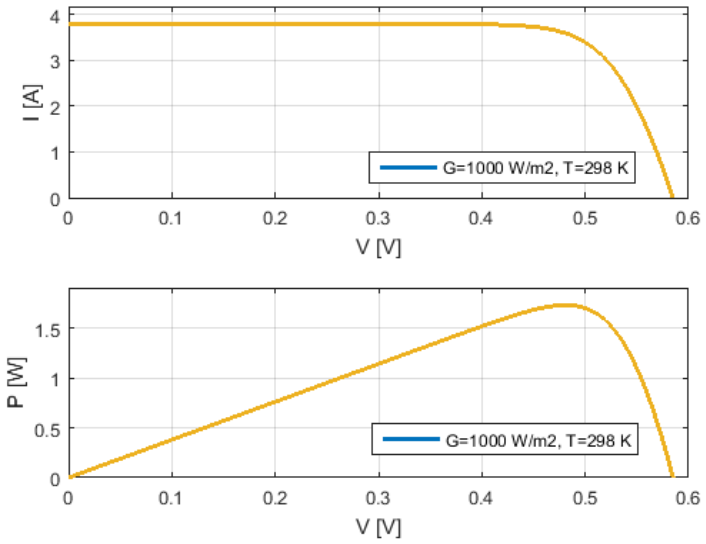

Figure 21. PV model characteristics V-I curves results

The necessary calculations of the solar panel numbers needed to get the desired demand power are shown below.

$I_m = 3.5\ A$

$V_m = 17.1\ V$

$P_m = 60\ W$

$V_{ref} = 300\ V$

$P_{ref} = 25\ kW$

$$n_s = \frac{Vref}{V_m} = \frac{300\ V}{17.1\ V} \rightarrow n_s = 17.5\ \approx 18$$

$$I_{ref} = \frac{P_{ref}}{V_{ref}} = \frac{25\ kW}{300\ V} = 83.33$$

$$n_p = \frac{I_{ref}}{I_m} = \frac{83.33\ A}{3.5\ A} \rightarrow n_p = 23.8\ \approx\ 24$$

Solar irradiance real data behavior in Mayaguez, Puerto Rico was used with the objective to get a similar performance of PV generation compared to a real system. The data used was measured in Luis A. Stefani Engineering Building in the University of Puerto Rico at Mayaguez (18°12'34.9"N - 67°08'21.6"W).

Running an experiment, the user has the option to choose the type of weather day that wants to use in the experiment. The options are: mostly sunny, partially sunny or cloudy.

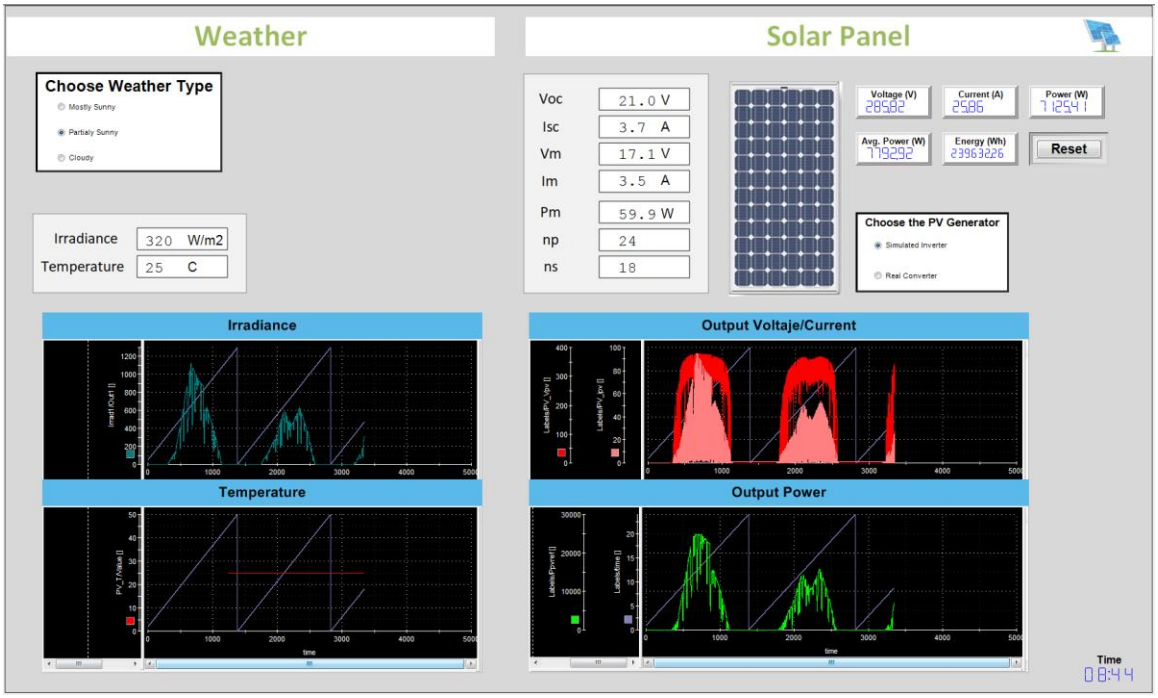

Figure 22. SCADA solar panel display

Figure 22 shows the corresponding display to the photovoltaic model behavior and operation. In the left side the display shows in real time the irradiance and temperature current values in simulation, also a trend graphic of the irradiance. In the right side, the main modeled solar panel characteristics, the output electrical parameters, and their trends are shown.

This solar panel was developed as a software modeled component but depending of the needs of the experiment, it could be replaced by another software modeled prime energy source or real hardware without modifying the entire structure or other components functionalities. This could be done because the implementation was based on the characterization and standardization of the inputs and outputs of each component carried out in the design phase. Some other solar panel mathematical models could be implemented based on [38], [44], [45]. Other type of software modeled prime energy

sources could be used as wind turbines [46] [47] [48] or solar thermal plants [49] [50] [51]. Real hardware also could be used to perform real generation. Some solar panel manufacturers are: Trina Solar, JinkoSolar, Canadian Solar, Solarex, SunPower, SolarTech. Some wind turbines manufacturers are: Enercon, Siemens, Sulzon Groups, General Electric, Gamesa, United Power.

6.3. Power Converter

The module used is a 2.2 kW Danfoss Drive reconfigured with a different control board to operate as a three phase DC-AC power converter. The converter has the enable and reset digital inputs, trip signal digital output, and PWM inputs for each phase. The PWM inputs allow to govern the IGBT gate driver depending of the control strategies implemented in the HIL device. Due to the photovoltaic generator modeled in this scenario have a power capability of 25 kW, the power reference of the real inverter was scaled to work up to 2.2 kW.

An LCL filter was connected to the inverter AC output to mitigate the harmonics generated by the switching in the inverter and leave only the fundamental frequency signal.

The voltage controller operates in cascaded control loop, i.e. an internal loop to control the current of the inductance and an external loop to control the voltage of the capacitor. The procedure to trade off the controller is presented in [52] that uses a Proportional-Resonant Control strategy. The main advantage of resonant control is its simplicity, although this is compromised when the design is performed to eliminate multiple harmonics. The control strategy used to command the inverter gates was not developed in this work, the control module was obtained from [52] and the loop constants was tuned to integrate the control with the plant. Figure 23 shows the graphical interface display used to operate the inverter and the synchronization with the grid.

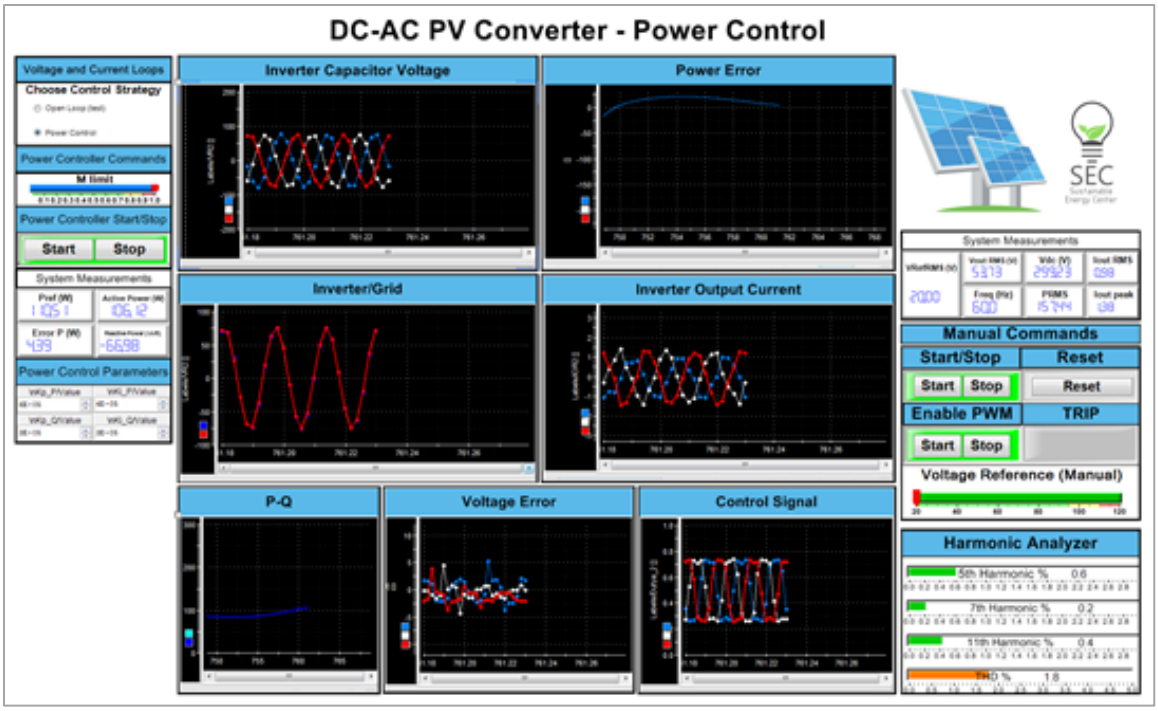

Figure 23. SCADA DC-AC power inverter display

To accomplish the connection between the inverter and the grid, a phase lock loop (PLL) was used to synchronize the signal generated by the inverter with the signal phase measured of the grid.

According to the hierarchical control model in Microgrids presented in the literature review, the control developed in the power converter belongs to the inner loops level.

This power converter was developed as a real hardware component but depending of the needs of the experiment could be replaced by another hardware device or a software simulated power converter without modifying the entire structure or other components functionalities. This could be done because the implementation was based on the characterization and standardization of the inputs and outputs of each component carried out in the design phase. Some software simulated converters topologies are presented in [53], [54], [55].

6.4. Storage System

This scenario uses a 15 kW electrical battery model based on a Thevenin circuit with two RC parallel branches, it is proposed in [41]. The model represents the behavior of a

stack of 210 Ni-Cd cells and 22 Ah of capacity. The change of the internal attributes due to variations in the internal and external variables are considered. Parameters as state of health (SOH) and cell temperature are not considered in the battery model used.

The model considers hysteresis effects during charging and discharging, including the transients between them. The State of Charge (SOC) of the battery is the quantity of charge remaining in the battery expressed in percentage with regard to the nominal capacity. This quantity is calculated by means of measuring battery current over the considered period of time.

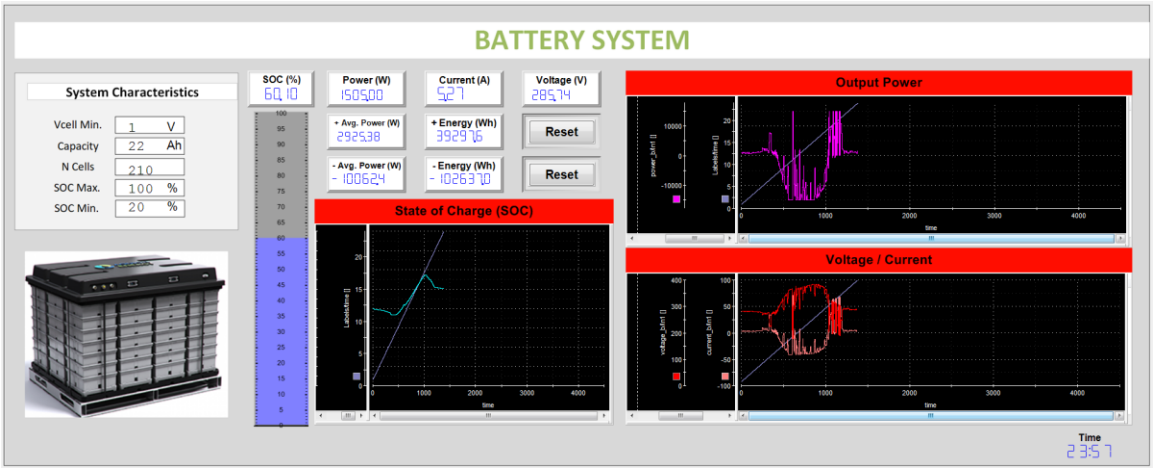

Figure 24. SCADA storage system display

Figure 24 shows the corresponding display to the battery model behavior. In the left side the display shows the main battery model parameters, the output electrical parameters of the model simulation (power, current, voltage, SOC) and their trends.

The battery module is a component used in MATLAB Simulink to construct the entire scenario obtained from [41] but was not developed by the author.

With the objective to protect the battery, a charge controller was implemented. The designed logic validates the SOC and the microgrid power demand to take actions. If the SOC of the battery is equal or greater than 80% and the microgrid is charging the battery, the charge controller disables the battery input power flow. If the SOC of the battery is equal or minor to 20% and the microgrid is demanding power from the battery, the charge

controller disables the battery output power flow. Other values in the battery parameters are considered as normal operational state.

The power converter related to the battery is considered as ideal converter, it means that the power consumed or delivered by the battery in DC is exactly the same in AC. It means that the DC power generated/demanded by the storage system is converted without losses to AC power.

This battery system was developed as a software modeled component but depending of the needs of the experiment, it could be replaced by another software modeled storage system or real hardware without modifying the entire structure or other components functionalities. This could be done because the implementation was based on the characterization and standardization of the inputs and outputs of each component carried out in the design phase. Some other software simulated storage systems were identified in [42], [56], [57].

6.5. Smart Meter

The implementation of the meter module was divided by the main functions of the smart meter. To accomplish the physical electrical measurements, a circuit board with voltage (LV25-P) and current (LA25-NP) sensors was constructed with the objective to acquire the signals with the analog dSPACE board. The analog dSPACE board channels are configured to read voltages scaled between -10Vdc and +10Vdc, with currents not higher than 10 mA. Figure 25 and Figure 26 shows the implemented sensor circuit to process the signals and deliver the voltage level needed in the channel.

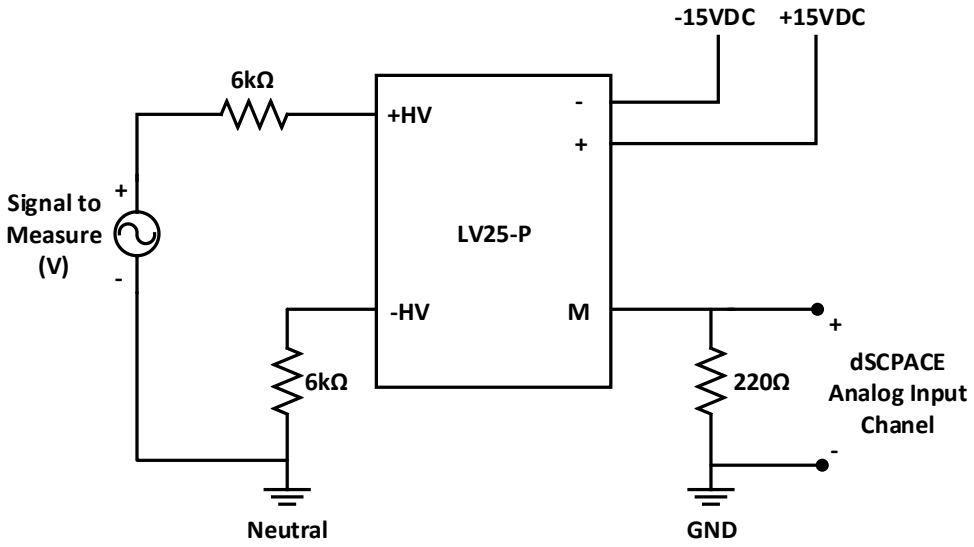

Figure 25. Voltage sensing circuit

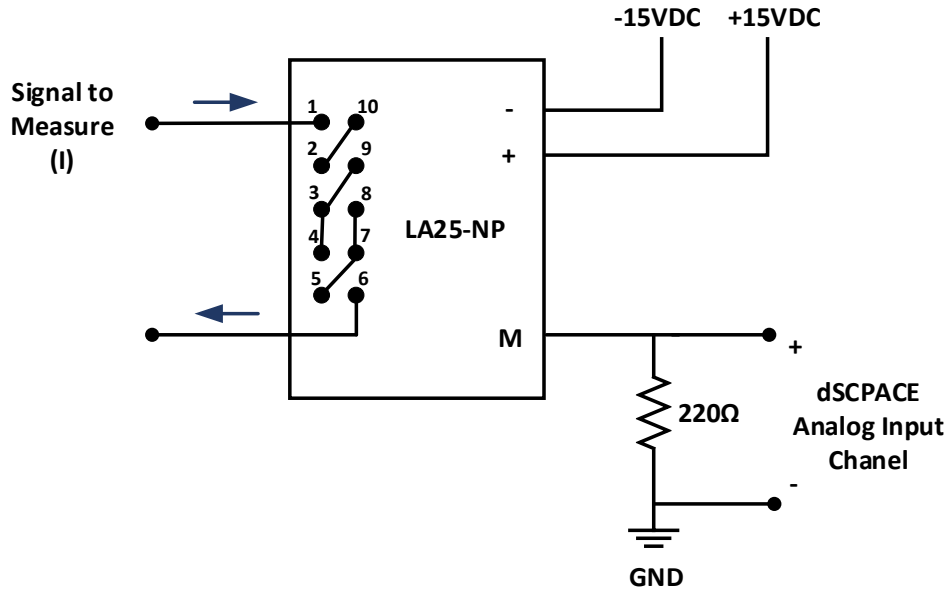

Figure 26. Current sensing circuit

The processing and communication functions was developed in the HIL device. Figure 27 shows the SCADA display with the measurements and calculated parameters in the application.

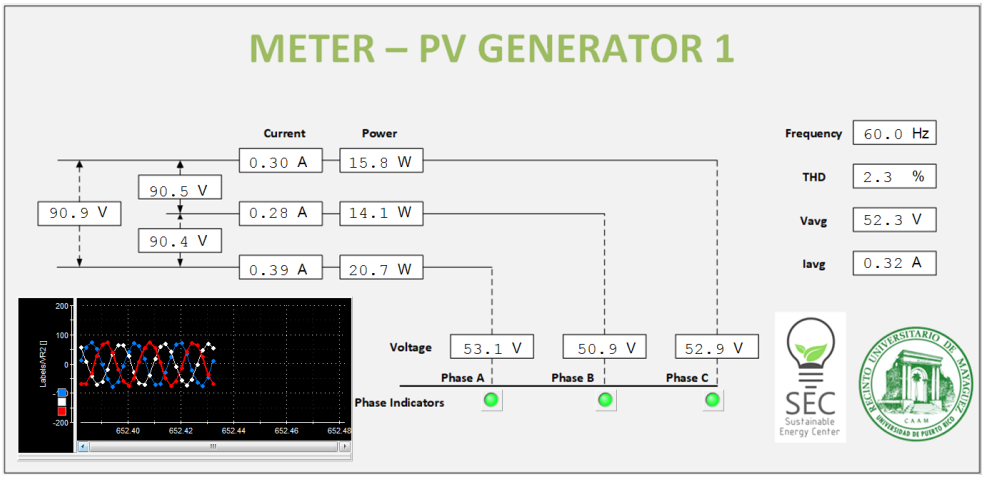

Figure 27. SCADA Smart meter display

The processing module developed include the calculations of active power, phase to phase voltage, frequency, total harmonic distortion (THD), average voltage and average current.

Data communication between the smart meter and other scenario components is considered as ideal conditions, it means that the regular AMI system communication delays are not considered. Real hardware could be used to implement an AMI system and perform a microgrid scenario in the HIL platform. Some identified works that implements AMI systems are presented in [19], [58], [59], [60].

This smart meter system was developed as a hybrid modeled-hardware component but depending of the needs of the experiment, it could be replaced by a software modeled component or a real hardware without modifying the entire structure or other components functionalities. This could be done because the implementation was based on the characterization and standardization of the inputs and outputs of each component carried out in the design phase. Some other smart meter implementation was identified in [33], [61], [62].

6.6. Residential Loads

A small community of three 10.3 kW residential loads was modeled. Power consumption behavior of the residential loads was modeled following similar conduct patterns of obtained consumption data from families in Puerto Rico.

The model includes three independent loads with the characterization of each internal home components with a base consumption rate and a random number component consumption to get a variation and different patterns in each residential component and experiment. Next, there is a table with the characterized component, power consumption and consumption schedule.

Table 3. Residential loads components consumption

Load Type	Power Consumption [W]	Active Schedule
Television 1	85	7 am - 2 pm / 6 pm - 11 pm
Television 2	70	8 am - 2 pm / 6 pm - 10 pm
Television 3	70	8 am - 2 pm / 6 pm - 10 pm
Refrigerator	250	12 am - 12 am
Air Conditioner	690	12 am - 12 am
Microwave	1,500	12 am - 1 pm / 7 pm - 8 pm
Oven	3,000	6 am - 7 am/ 11 am - 1 pm / 6 pm - 9 pm
Coffee Machine	600	5 am - 2 pm / 4 pm - 9 pm
Washing Machine	2,000	6 pm - 10 pm
Drying Machine	1,800	6 pm - 10 pm
Interior Lights	150	4 am - 7 am / 6 pm - 12 am
External Lights	150	6 pm - 7 am
Total	**10,365**	

The loads behavior modeled does not have discrimination between week days and weekend days.

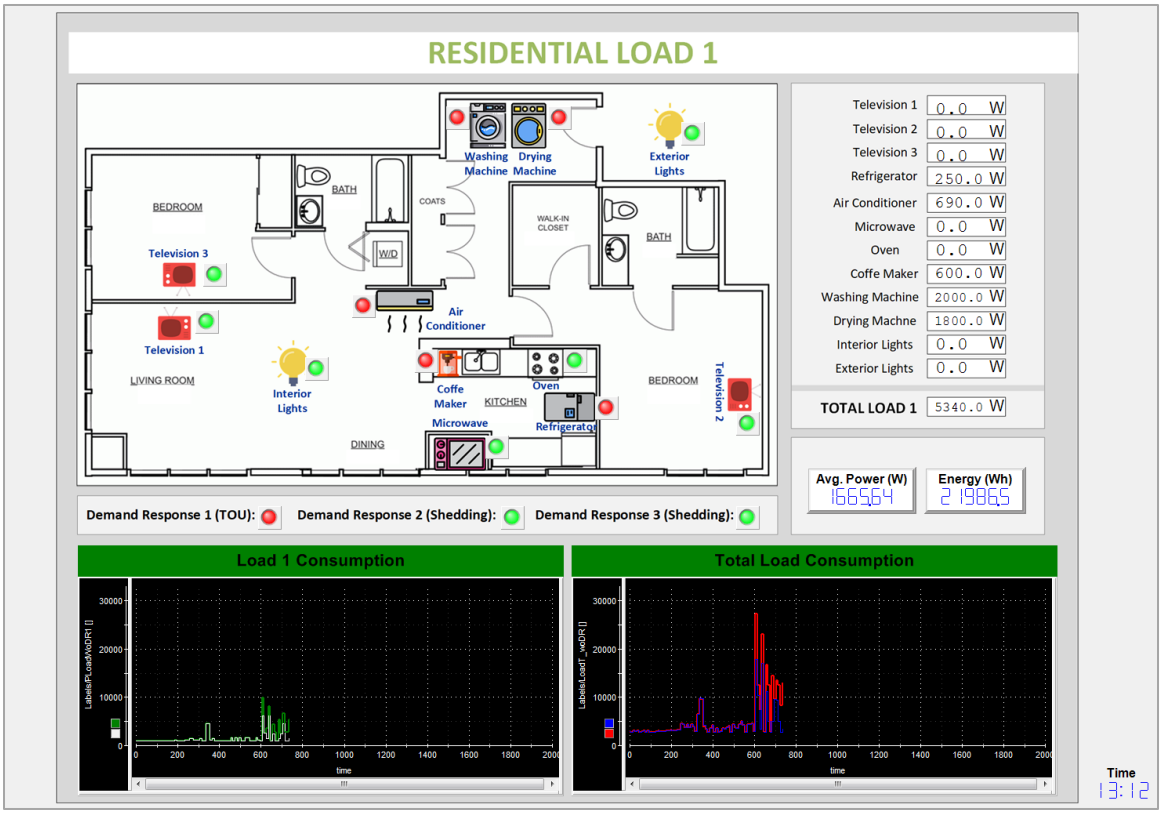

Figure 28. SCADA residential load display

Figure 28 shows the display of a residential load. The display shows the power consumption values of the residential components and the trend consumption of each house in real time.

This residential load was developed as a software modeled component but depending of the needs of the experiment, the quantity of loads could be incremented/decreased or replaced by another software modeled load (residential, commercial, industrial) or real hardware without modifying the entire structure or other components functionalities. This could be done because the implementation was based on the characterization and standardization of the inputs and outputs of each component carried out in the design phase. Some other load implementation works were identified in [63], [64], [65].

Another feature that could be implemented related to the loads is to implement the behavior dependences that the energy consumption actually has depending of the size of

the family, day of the week (weekday or weekend), the weather (sunny, cloudy, rainy, snowy) or the power generation prediction according to the weather.

6.7. Microgrid

In this scenario, the Microgrid is considered as an ideal common node where all the generators, storage systems, loads and grids are connected.

The microgrid and utility grid components in this scenario were developed as ideal components but depending of the needs of the experiment this component could be replaced by a more complex grid models or real hardware without modifying the entire structure or other components functionalities. This could be done because the implementation was based on the characterization and standardization of the inputs and outputs of each component carried out in the design phase. Some distribution and transmission models that could be implemented in the platform were identified in [66], [67], [68], [69].

6.8. EMS

A fuzzy logic controller (FLC) is developed to accomplish the control objective of the experiment. The FLC is designed to maintain a constant flow from the electrical grid, preserving the stability of the grid keeping a flat power demand and to maximize the energy produced by the PV generator. EMS sets a power reference to the storage system depending of the power needed in the grid to supply the loads. Other important function of the control is to keep the SOC of the battery between 30% and 80%.

The FLC was developed in the Fuzzy Logic Designer MATLAB Toolbox. The system has two input variables: the SOC and the power current value of the battery (BattPower).

The power balancing equation in the microgrid is presented below:

$$BattPower = PL1 + PL2 + PL3 - PV - PGrid$$

SOC variable is defined with a value between 0 and 100. This variable is represented by the following levels: Low Soc (L), Medium Low (ML), Medium (M), Medium High (MH) and High (H). In

Level	Name	Function Type	Parameters
Low SOC	L	Trapezoidal-shaped	[0 0 30 40]
Medium Low SOC	ML	Triangular-shaped	[35 42.5 50]
Medium SOC	M	Triangular-shaped	[45 55 65]
Medium High SOC	MH	Triangular-shaped	[60 68.5 75]
High SOC	H	Trapezoidal-shaped	[70 80 100 100]

Table 4 and Figure 29Figure 1, the definition and variable membership input function are shown.

Table 4. SOC fuzzy membership function

Level	Name	Function Type	Parameters
Low SOC	L	Trapezoidal-shaped	[0 0 30 40]
Medium Low SOC	ML	Triangular-shaped	[35 42.5 50]
Medium SOC	M	Triangular-shaped	[45 55 65]
Medium High SOC	MH	Triangular-shaped	[60 68.5 75]
High SOC	H	Trapezoidal-shaped	[70 80 100 100]

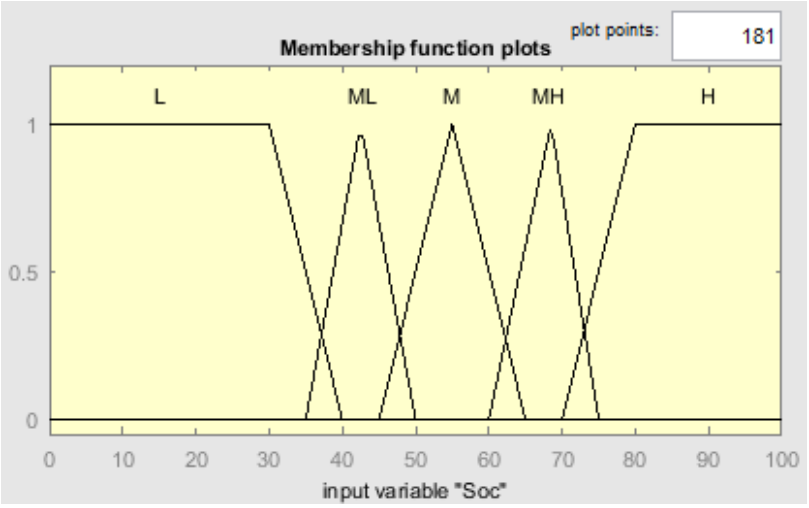

Figure 29. SOC fuzzy membership function

BattPower variable is defined with a value between -15,000 and 15,0000. The negative part of BattPower means that the battery is consuming power to increase the charge and the positive part means that the battery is delivering power to the microgrid. This variable is represented by the following levels: High Negative (-)H, Medium Negative

(-)M, Low Negative (-)L, Low Positive (+)L, Medium Positive (+)M, and High Positive (+)H. In Table 5 and Figure 30, the definition and variable membership input function are shown.

Table 5. BattPower fuzzy membership function

Level	Name	Function Type	Parameters
High Negative BattPower	(-)H	Trapezoidal-shaped	[-15000 -15000 -11000 -9000]
Medium Negative BattPower	(-)M	Triangular-shaped	[-10000 -7000 -4000]
Low Negative BattPower	(-)L	Triangular-shaped	[-5000 -2500 500]
Low Positive BattPower	(+)L	Triangular-shaped	[-500 2500 5000]
Medium Positive BattPower	(+)M	Triangular-shaped	[4000 7000 10000]
High Positive BattPower	(+)H	Trapezoidal-shaped	[9000 1100 15000 15000]

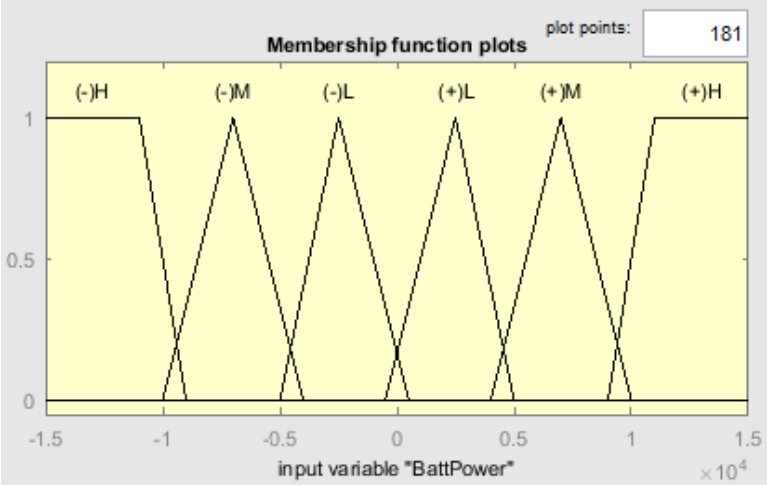

Figure 30. BattPower fuzzy membership function

The outputs variables of the FLC are three levels of Demand Response digital commands. DR1 executes an incentive based TOU program that re schedule the used the washing and drying machine loads from the night to the middle day hours to take advantage of the peak PV generation at this hours. DR2 is a command that allows a low level of Demand Response through load shedding of some non-critical loads (exterior lights) and DR3 executes the shedding of all the non-critical residential loads (air conditioner).

The Fuzzy Inference System (FIS) used to get the output functions is the Mamdani's direct method. The rules related to each combination of the function is specified in Appendix B.

According to the hierarchical control model in Microgrids presented in the literature review, the control developed in the power converter belongs to the tertiary control level.

6.9. Complete Scenario

Figure 31 shows the conceptual model of the implemented scenario. The light blue modules represent the software modeled modules and the green modules, and the dark green modules are the real hardware components used in the scenario. The light blue variables are parameters that are simulated and distributed by software. The dark green variables are parameters physically measured by the platform and connected internally by software with the other modules. Each module represented in the diagram could be replaced by a different software modeled component or the real hardware component without modifying the entire structure or other components. This could be done because the implementation was based on the characterization and standardization of the inputs and outputs of each component carried out in the design phase.

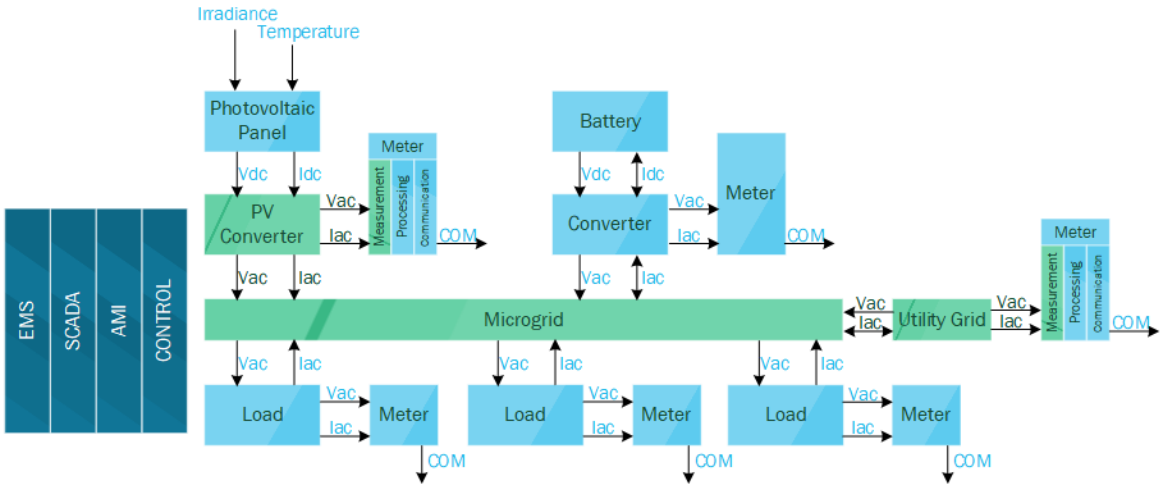

Figure 31. Developed Scenario Conceptual Model

Figure 32 represents the HIL electrical diagram of the developed scenario. At the left of the diagram, the software modeled components are shown. As described previously, the simulated models and data behavior are the solar irradiance, solar panel, battery

system, and residential loads. At the right of the diagram, the hardware configuration and electrical components are shown. The hardware implementation includes a fixed DC source, inverter, LCL filter, measurement boards, connection switch, and an isolation transformer. As shown in the figure, the interaction between the solar panel and MPPT with the inverter is the power reference delivered through the control. The output interaction between the control and the inverter is made between the control commands as enable, reset, and PWM signals per phase. The inverter feedback includes the inverter trip signal, the internal filter current, capacitor voltage, and output filter current.

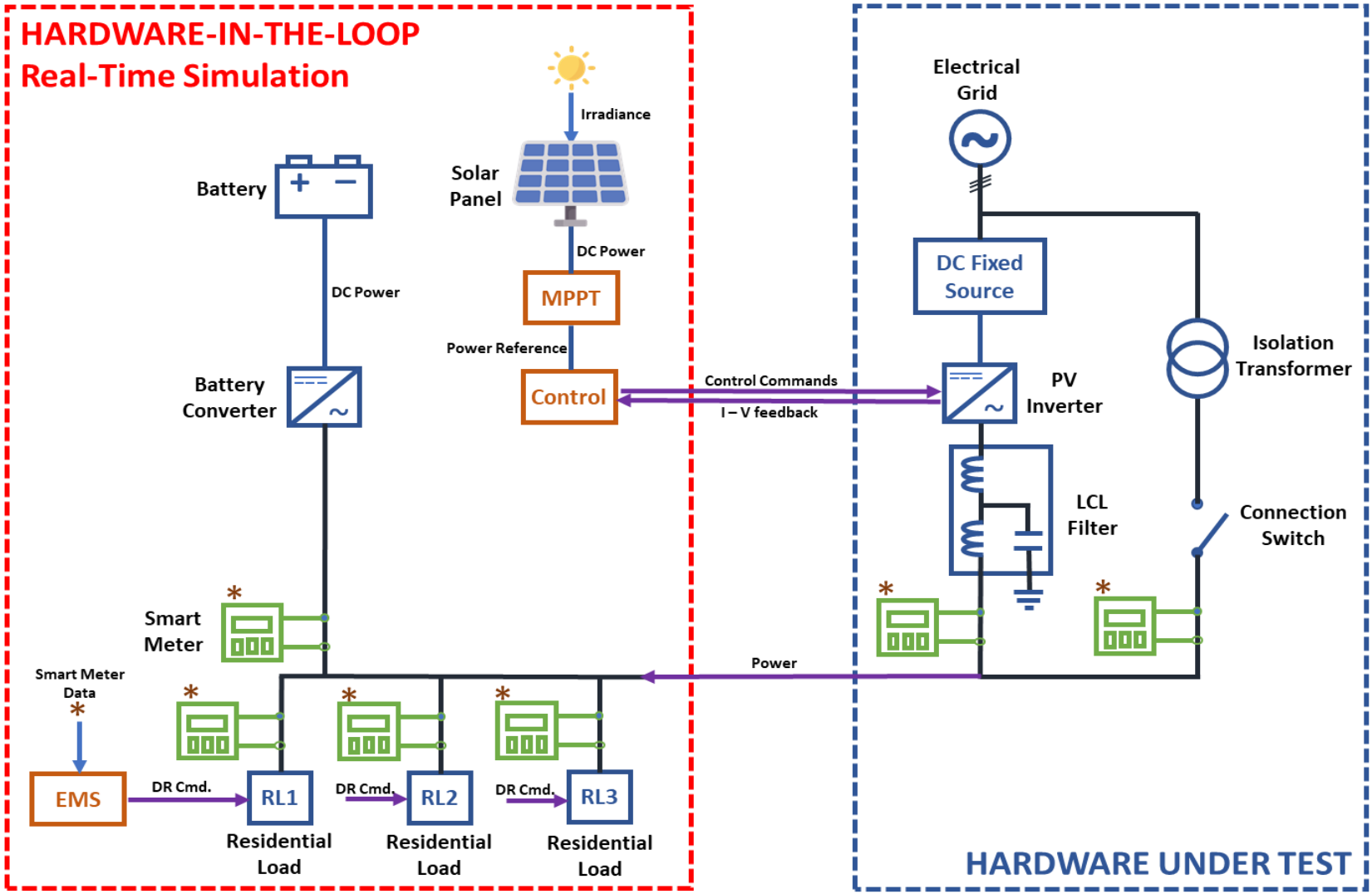

Figure 32. Hardware-in-the-Loop Developed Scenario Electrical Diagram

Chapter 7

SCENARIO SIMULATION RESULTS AND ANALYSIS

Following the conceptual system overview, this chapter presents the results obtained from each component and an entire scenario experimentation. All presented results were obtained from the executed experiments in dSPACE ControlDesk. Each experiment result is composed by a graphical trend and a data table with the numerical results. In the graphical trend each unit of x-axes represent 1 minute, then 1440 units represent 1 day in the experiment.

7.1. Solar Panel

In this experiment, the solar panel model was simulated with three different irradiance pattern per day as input. First day was simulated as a mostly sunny day, second day as partially sunny and third day as a cloudy day. The graphical results of simulation are shown in Figure 33.

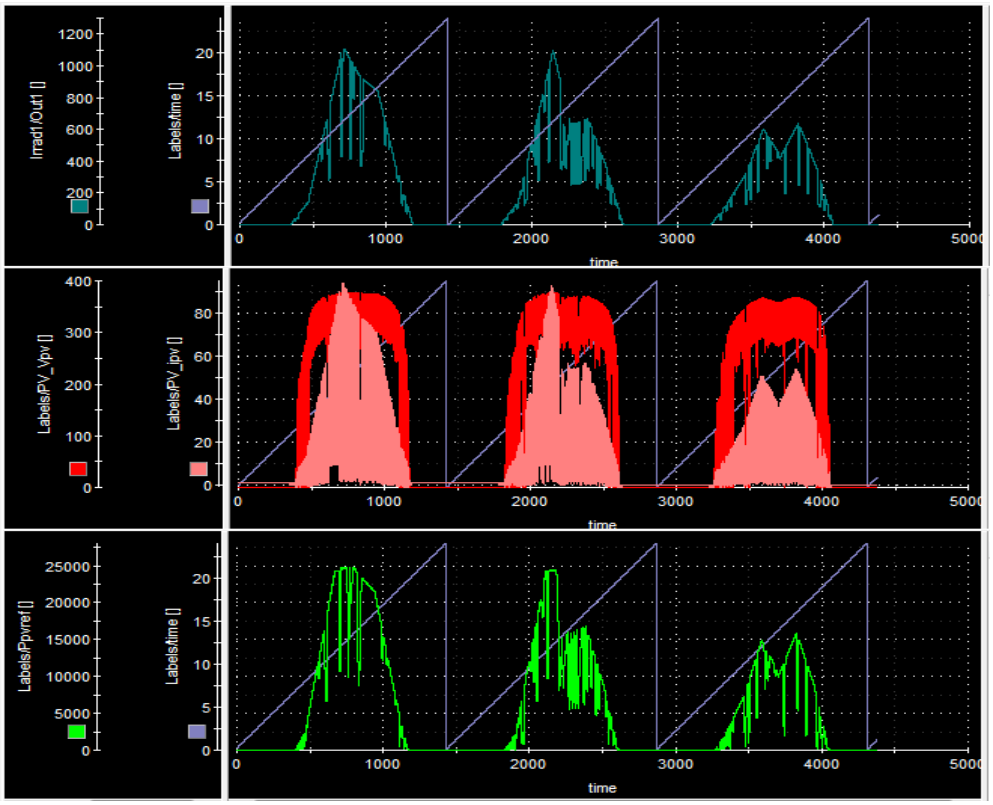

Figure 33. Solar Panel model simulation results

Each trend has in purple line that represents the time of the day (from 0 hours at the lower point to 24 hours at the highest point). The top trend in the figure shows the irradiance behavior. It graphically shows the different type days in the simulation, the difference between the peaks and sun hours in the day are well represented. The middle trend shows the solar panel output voltage and current. The constant movement of the voltage and current values represent the MPPT work that is always looking for the maximum power point in the panel curve when the input irradiance changes. The bottom trend shows the solar panel output power. Represented by the green line, the output power follows a similar behavior of the irradiance.

Table 6. Solar panel model simulation results

	Day 1	Day 2	Day 3
Max. Irradiance Peak [W/m2]	1,095	1,094	635
Avg. Irradiance [W/m2]	670	588	417
Max. Power Peak [W]	24,755	24,361	15,408
Avg. Power [W]	11,796	7,284	6,587
Generated Energy [Wh]	165,341	102,105	92,332

Table 6 shows the main numeric inputs and results of the solar panel experiment. The maximum irradiance peaks were registered around midday. The data to the averages calculations was registered only between 6 am and 8 pm. Numerical data in Table 6 confirm the energy production difference between the three days.

The results obtained in this experiment are similar to the results that the author present in the work [37]. This is because of the near behavior of the solar panel curves and the maximum power point tracking in comparison with the manufacturer solar panel curves presented in the component data sheet and the paper results. This results demonstrate the adequate response of the solar panel component in the scenario.

7.2. Power Converter

The physical inverter experiment begins with the power reference delivered by the MPPT to the inverter control. The inverter is physically supplied by a DC source with 300 Vdc. The inverter output is connected to the power grid through an AC switch that is closed when the control confirms that the generated voltage is synchronized with the grid

voltage with the PLL. The generated power in the experiment flows from the inverter to the grid. To get a different PV generation behavior, the solar panel model was simulated with three different irradiance pattern per day: mostly sunny, partially sunny and cloudy. Figure 34 shows the PV inverter graphical results.

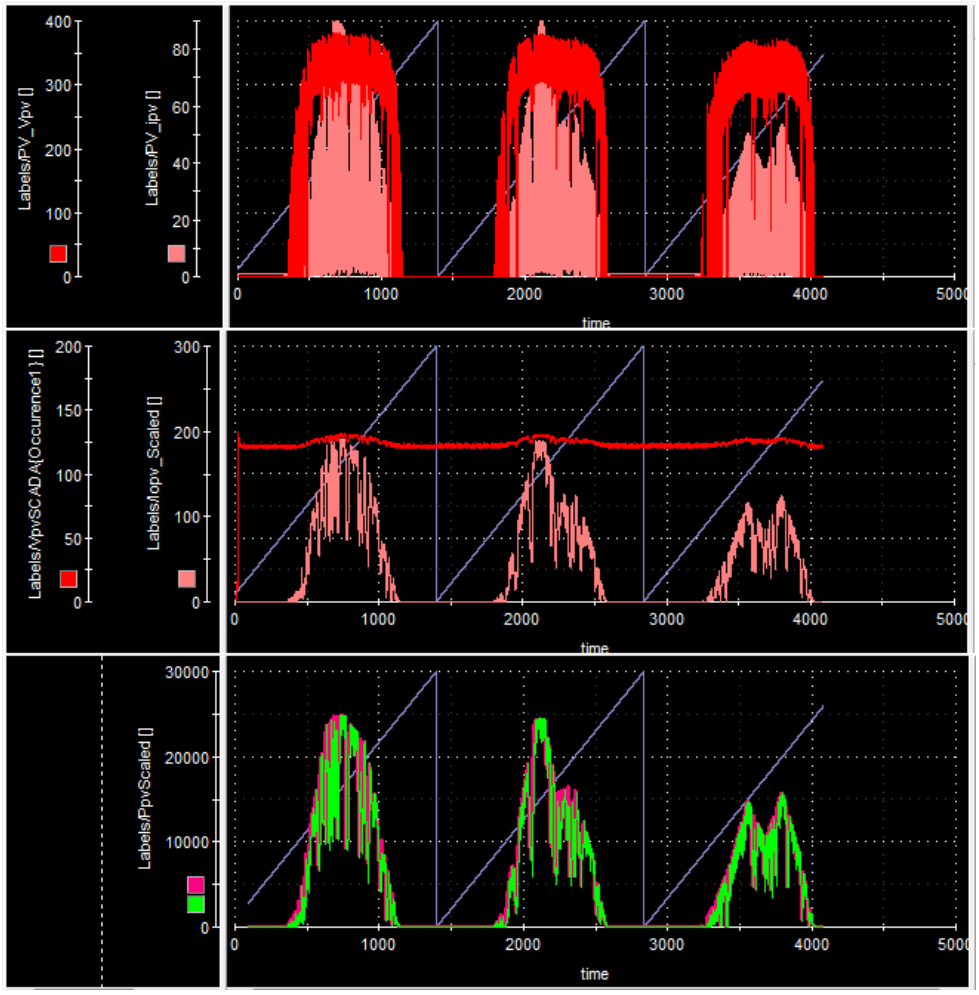

Figure 34. PV with power converter simulation results

Top trend in the figure shows the input DC voltage (red line) and current (pink line) obtained from the solar panel. Middle trend represents the AC voltage (red line) and current (pink line) generated by the inverter. According to the control and PLL, the inverter output voltage (red line) is always close to the grid amplitude, 120V rms. The bottom trend shows the power reference (fuchsia line) and the inverter output power

(green line). The inverter output follows in most of the simulation the reference values, but there are sometimes that the inverter does not reach the reference power.

Table 7 shows the numerical results of the experiment. The numerical results confirm that there are power losses in the power conversion process. The best energy conversion rate comparing the inverter generated energy with the solar panel generated energy in the simulated three days was 0.981.

Table 7. PV with power converter simulation results

	Day 1	Day 2	Day 3
Max. PV Power Peak [W]	24,771	24,375	15,762
Max. Inverter Power Peak [W]	24,771	24,375	15,762
Avg. PV Power [W]	9,992	7,289	6,462
PV Generated Energy [Wh]	140,061	102,168	90,587
Avg. Inverter Power [W]	9,749	7,094	6,340
Inverter Generated Energy [Wh]	136,652	99,438	88,869
Energy Conversion Rate	0.976	0.973	0.981

7.3. Residential Loads

The loads behavior modeled has a fixed component that depends of the data consumption specified in section 8 and a variable component that depends of the time of the day and a random number. Figure 35 shows the result behavior of the loads in one day. The total load behavior (red line) shows three power peaks in one day. It occurs in the morning when the people awake in the house, near to midday while they cook the lunch and eat it, and in the night when the people arrives to the house from work or study until they go to sleep.

Table 8 shows the numerical results of the residential loads experiment. The major power consumption peak was found in the night.

Table 8. Residential load model simulation results

	Morning Peak Power [W]	Afternoon Peak Power [W]	Night Peak Power [W]	Average Power [W]	Energy Consumption [Wh]
House 1	4,840	4,165	10,215	1,994.82	47,876
House 2	4,840	6,195	10,215	1,786.25	42,870
House 3	4,690	5,525	10,280	1,778.22	42,678
Total Load	1,120	13,770	28,125	5,559.29	133,424

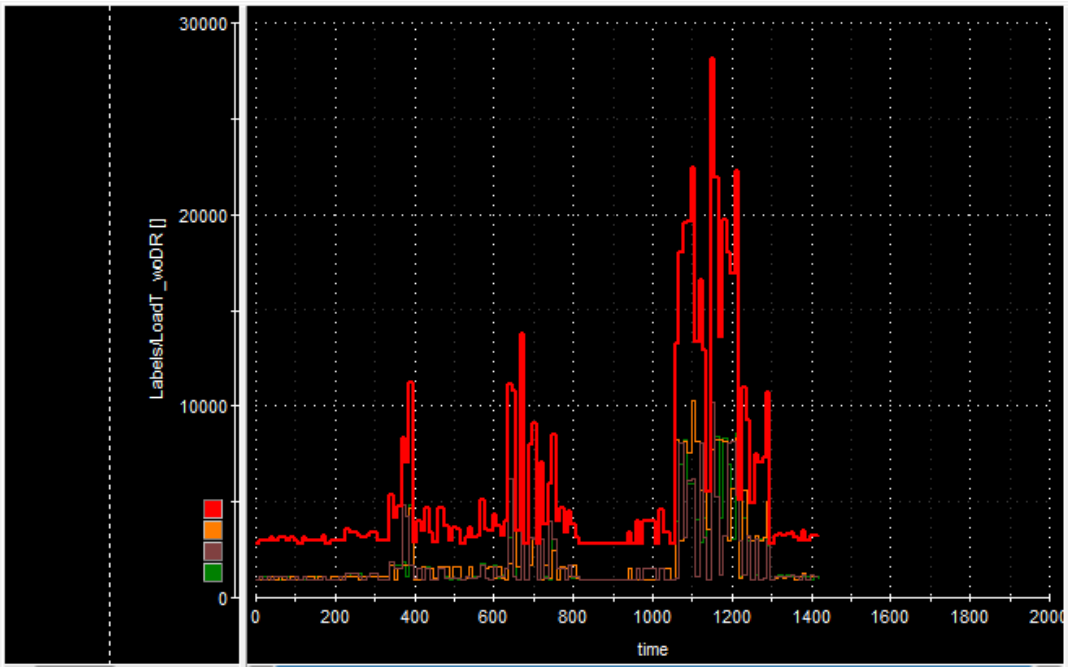

Figure 35. Residential load model simulation results – Total power consumption

Figure 36 shows the different behavior patterns of each house. Each residential load keeps the morning, afternoon and night pattern described before.

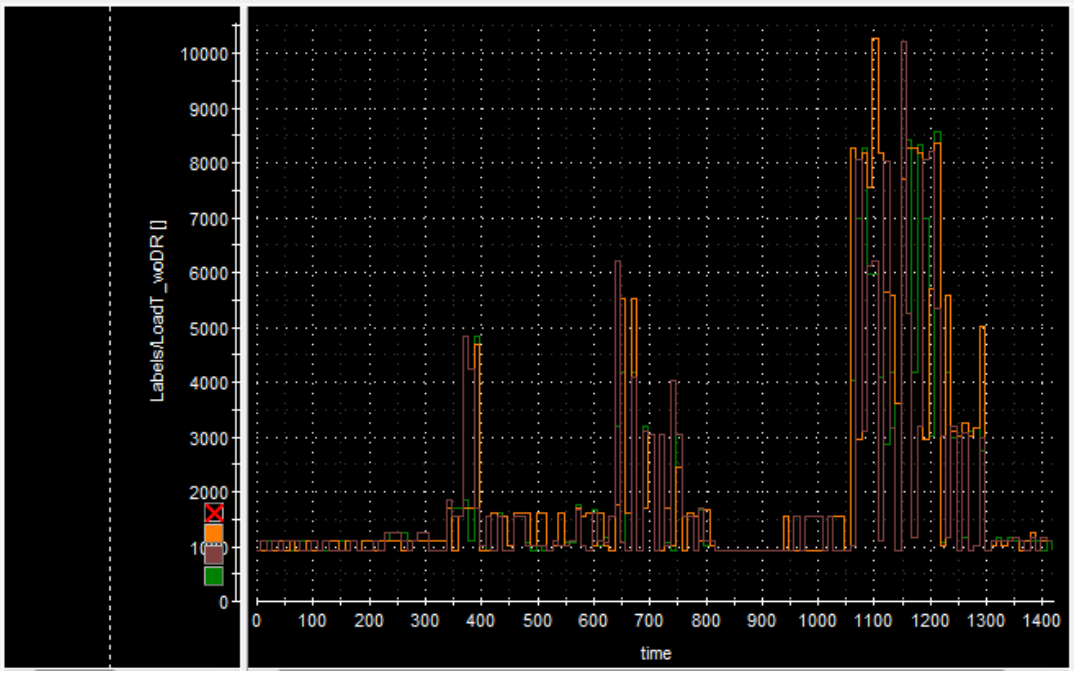

Figure 36. Residential load model simulation results – Individual power consumption

7.4. Battery System

The battery system experiment was divided in two parts. First, the battery was tested connected with the solar panel power generation. To get a different PV generation behavior, the solar panel model was simulated with three different irradiance pattern per day: mostly sunny, partially sunny and cloudy. Figure 37 shows the battery behavior when the solar panel generates power and charge the battery. The battery voltage (red line) and current behavior (pink line) are shown in top trend graphic. The SOC of the battery (aqua blue line), PV power (green line), and battery power (purple line) are shown in bottom trend.

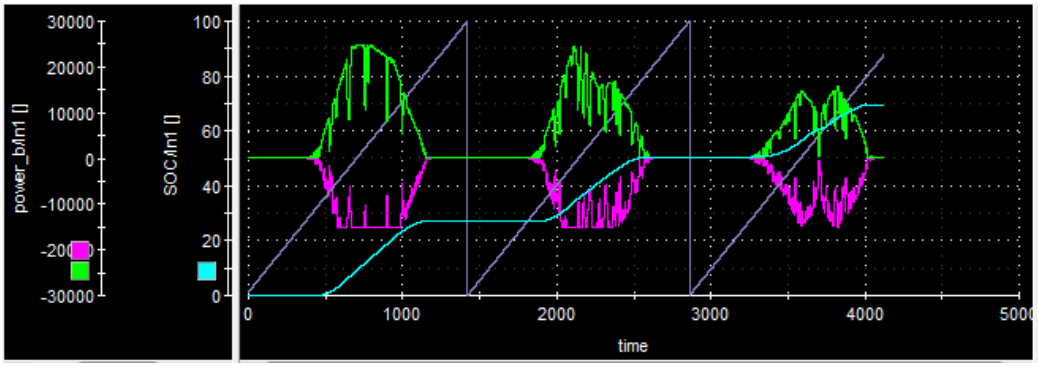

Figure 37. Battery model simulation results in charging cycle with PV generation

Table 9 shows the charging experiment numerical results. The charged energy in battery is minor compared to the PV generated energy due to the different power capacities of the components. The battery SOC in the experiment begins in 0% and after three days finished in 69.63%. As expected, the SOC had a major increase in a sunny day followed by the partially sunny day.

Table 9. Battery model simulation data results in charging cycle with PV generation

	Day 1	Day 2	Day 3
Max. PV Power Peak [W]	24,756	24,347	15,821
Max. Battery Power Peak [W]	15,000	15,000	15,000
Avg. Inverter Power [W]	-11,871	-8,957	-6,431
Inverter Generated Energy [Wh]	166,404	125,558	90,143
Avg. Battery Power [W]	-9,265	-8,134	-6,425
Battery Received Energy [Wh]	129,874	114,016	90,066
Charging %	27.1	23.48	19.05

The second experiment performed with the battery represents the discharge cycle. The battery was connected to the modeled residential load. Figure 38 shows the experiment graphical results. The SOC in the experiment begins in 55% and after the day finished in 41.1%. Different inclination levels of the SOC depending of the load consumption are shown in the trend.

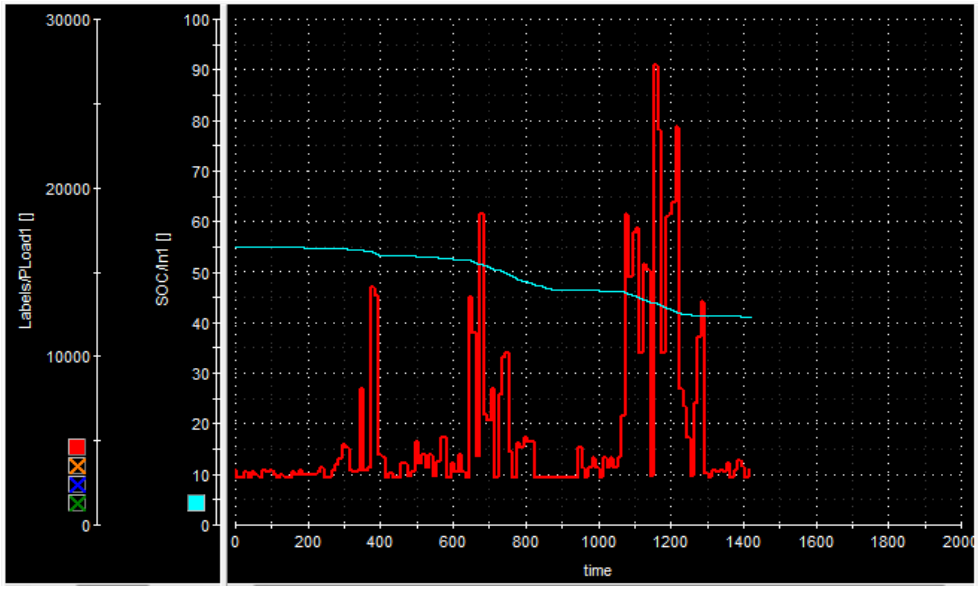

Figure 38. Battery model simulation results in discharging cycle with residential loads

Table 10. Battery model simulation results in discharging cycle

Morning Peak Power [W]	14,070
Afternoon Peak Power [W]	18,445
Noon Peak Power [W]	27,285
Average Power Consumption [W]	5,558
Total Energy Consumption [Wh]	133,424
Discharge %	13.9

The results obtained in this battery experiment are similar to the results that the author present in the work [41]. This is because of the near behavior of the battery SOC parameter in comparison with the SOC charging and discharging curves presented in the paper results. This results demonstrate the adequate response of the battery component in the developed scenario.

7.5. EMS

To test the different DR commands in the scenario, three independent experiments was performed. Each DR command was tested while the other commands was disabled with the aim to get independent DR performances.

7.5.1. Demand Response 1: Time of Use

The first experiment to test the DR1 TOU command includes the battery as power source and the residential loads for one day. The SOC of the battery begins in 55% and the battery supply the load power consumption all day in the experiment. Figure 39 shows the experiment graphical trends. The battery SOC (aqua line), real residential load (red line), and residential load without DR (blue line) are shown in the trend.

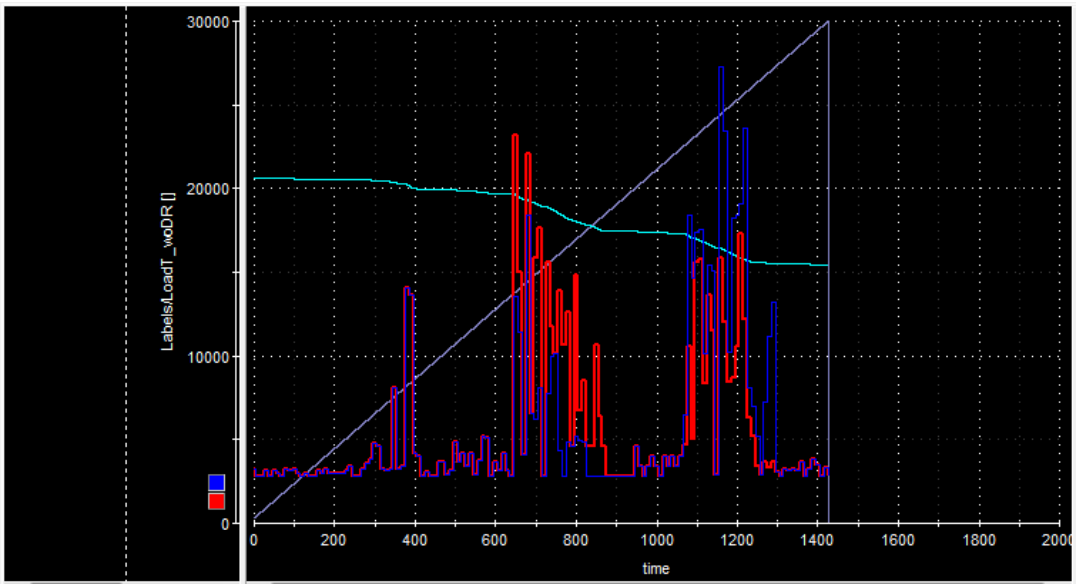

Figure 39. EMS - DR1 Time of Use command simulation results with residential loads

Due to the SOC of the battery is reduced and arrives to the medium level, the TOU DR command is activated. The activation of the DR command causes that the use of the washing and drying machine to be rescheduled from the night to the midday. Figure 39 shows that the higher power peak of the real power load is now occurring in the afternoon, and a lower power peak in the night. Table 11 confirms with numeric values the difference between the power peak between the afternoon and night. The average power (5,559 W) and total energy delivered (133,424 Wh) was equal in the real load and

load without DR consumption. This TOU DR program does not a direct energy savings impact but allows the system to take advantage the solar energy production in day light hours and to not use the battery neither the grid to supply high power peaks in the night.

Table 11. EMS - DR1 Time of Use command simulation results

	Morning Peak Power [W]	Afternoon Peak Power [W]	Night Peak Power [W]
Real Load	14,070	23,155	17,305
Load Without DR 1	14,070	18,445	27,285

The results obtained in this DR are similar to the results that the author present in the work [33]. This is because of the near behavior of the loads consumption after the consumption reschedule due to the DR TOU command activation in comparison with the consumption curves presented in the paper results. This results demonstrate the adequate response of the DR 1 – TOU program in the developed scenario.

7.5.2. Demand Response 2: Low Level Load Shedding

The experiment to test the DR2 load shedding is composed by the PV generator, the battery, and the residential load. The SOC of the battery begins in 55% and the PV production is configured as a sunny day. Figure 40 shows the experiment graphical trends. The battery SOC (aqua line), PV generator power (green line), battery power (fuchsia line), real residential load (red line), and residential load without DR (blue line) are shown in the trend.

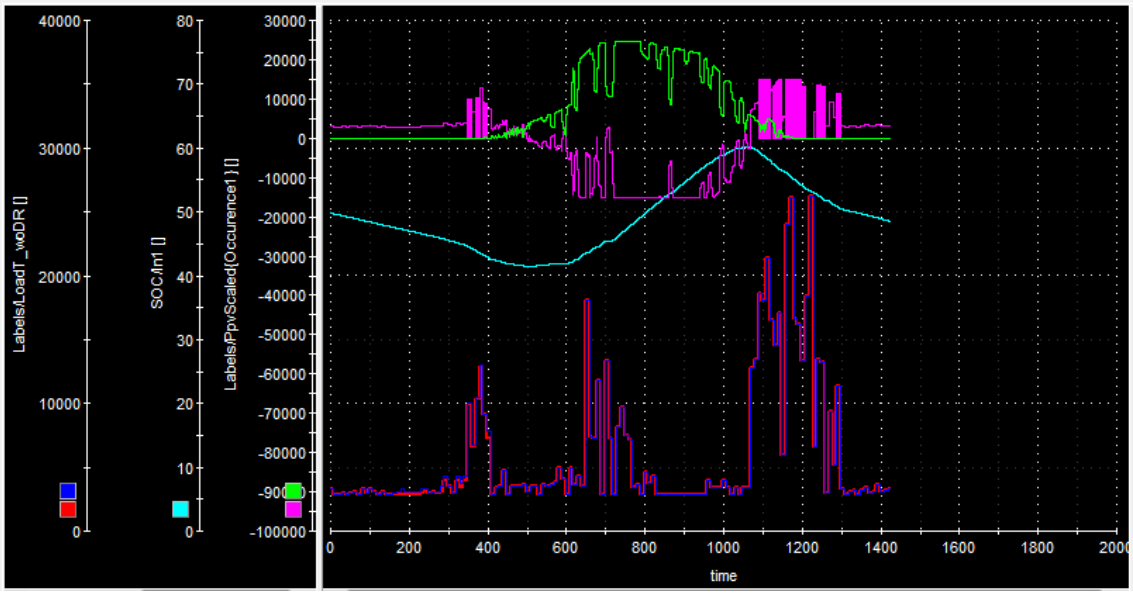

Figure 40. EMS - DR2 load shedding command simulation results with residential loads

The experiment begins with the battery supplying the power to the residential loads. Near to minute 152 a medium low SOC level is detected, due to the battery is supplying power, the DR2 command is activated. This command disconnects the external lights to optimize the power supplied by the battery in a low level. Due to the DR2 command only acts over the external lights, the energy savings effect just can be identified between 6pm and 7pm, when the external lights are on. The PV generator charge the battery during the day light and increase the battery SOC level deactivating the DR2 command. This is the reason why the DR2 program is not active at the night. Figure 41 shows a graphical zoom in the time when the DR2 command takes action.

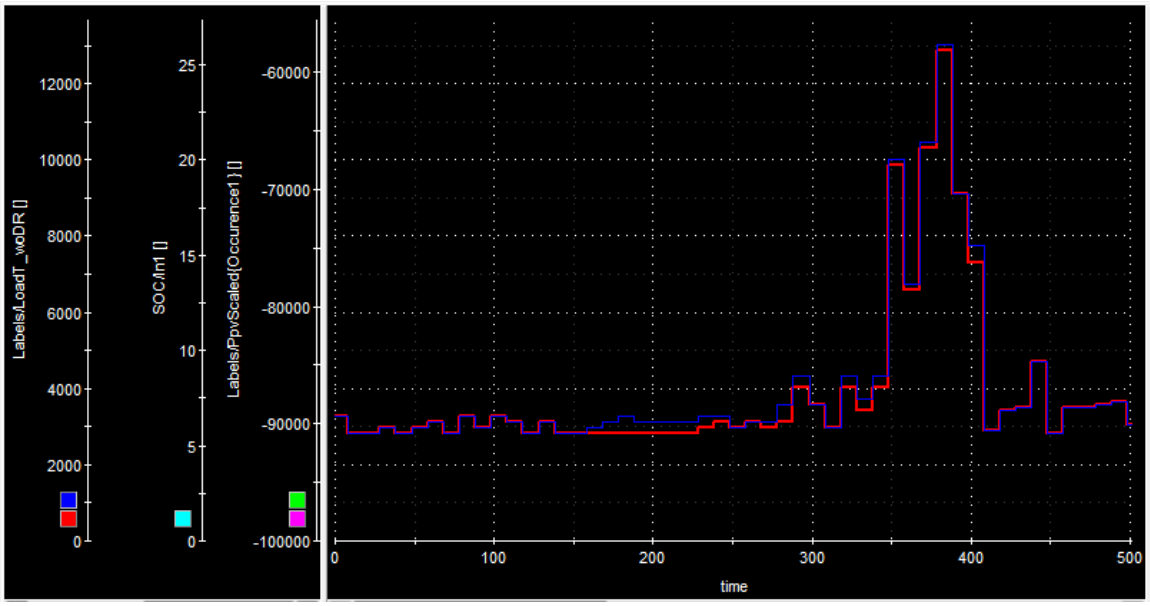

Figure 41. EMS - DR2 power consumption comparison

Table 12 shows the numerical results of the experiment. The data obtained reflects the graphical analysis, because the savings obtained with DR2 command active for 4.5 hours represent the 0.6% of the load regular energy consumption and power peaks in one day.

Table 12. EMS - DR2 load shedding command simulation results

	With DR2	Without DR2	Savings
Average Power House 1 [W]	1,931	1,945	14
Average Power House 2 [W]	1,948	1,958	10
Average Power House 3 [W]	1,938	1,952	14
Average Power Total Load [W]	5,817	5,855	**38**
Energy Consumption House 1 [Wh]	46,367	46,694	327
Energy Consumption House 2 [Wh]	46,755	47,005	250
Energy Consumption House 3 [Wh]	46,523	46,851	328
Total Load Energy Consumption [Wh]	139,645	140,550	**905**

The results obtained in this DR are similar to the results that the author present in the work [70]. This is because of the near behavior of the loads consumption after the load shedding due to the DR command activation in comparison with the consumption curves presented in the paper results. This results demonstrate the adequate response of the DR 2 – TOU program in the developed scenario.

7.5.3. Demand Response 3: Moderated Level Load Shedding

The experiment to test the DR3 load shedding is composed by the PV generator, the battery, and the residential load. The SOC of the battery begins in 55% and the PV production is configured as a sunny day. Figure 42 shows the experiment graphical trends. The battery SOC (aqua line), PV generator power (green line), battery power (fuchsia line), real residential load (red line), and residential load without DR (blue line) are shown in the trend.

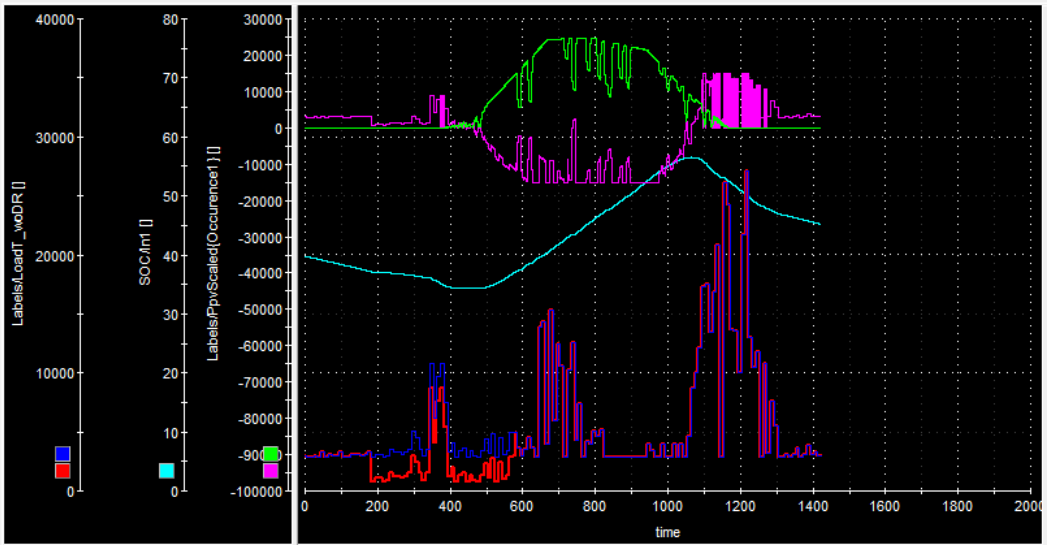

Figure 42. EMS - DR3 load shedding command simulation results with residential loads

The experiment begins with the battery supplying the power to the residential loads. Near to minute 165 a low SOC level is detected, then the DR3 command is activated. This command disconnects the air conditioner to optimize the power supplied by the battery in a moderated level. The DR3 command remains active until the PV generator charges the battery and increase the SOC at least to a medium low level. The rest of the day the SOC remains in acceptable levels. Figure 43 shows a graphical zoom in the time when the DR3 command takes action.

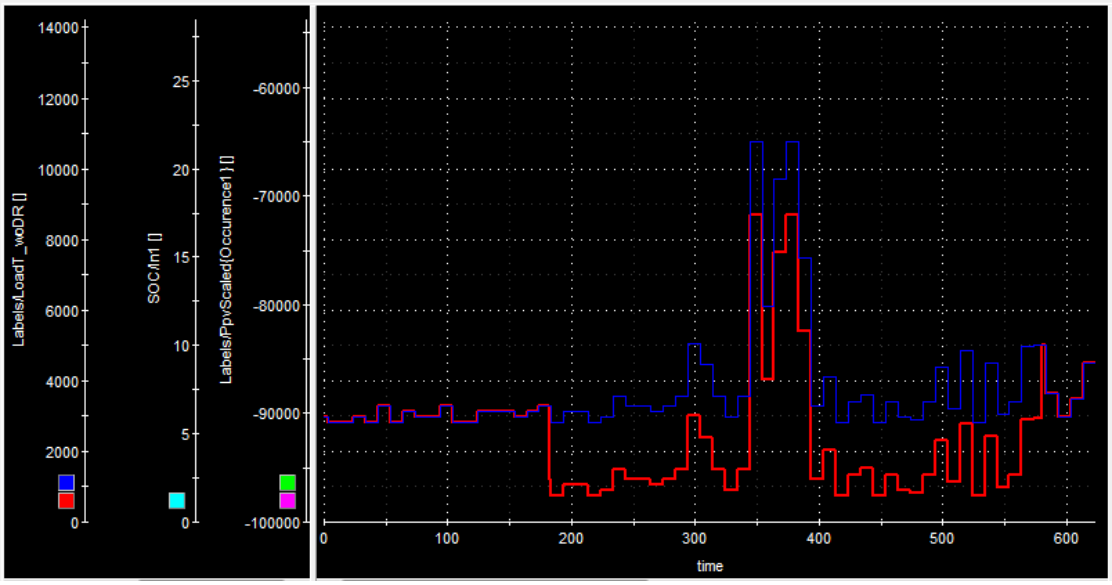

Figure 43. EMS - DR3 power consumption comparison

Table 13 shows the numerical results of the experiment. The data obtained reflects the graphical analysis, because the savings obtained with DR3 command active for 6.6 hours represent 10% of the load regular energy consumption and power peaks in one day.

Table 13. EMS - DR3 load shedding command simulation results

	With DR2	Without DR2	Difference
Average Power House 1 [W]	1,675	1,866	191
Average Power House 2 [W]	1,646	1,838	192
Average Power House 3 [W]	1,820	2,011	191
Average Power Total Load [W]	5,141	5,715	574
Energy Consumption House 1 [Wh]	40,208	44,797	4,589
Energy Consumption House 2 [Wh]	39,524	44,113	4,589
Energy Consumption House 3 [Wh]	43,696	48,284	4,588
Total Load Energy Consumption [Wh]	123,428	137,194	13,766

The results obtained in this DR are similar to the results that the author present in the work [70]. This is because of the near behavior of the loads consumption after the load shedding due to the DR command activation in comparison with the consumption curves presented in the paper results. This results demonstrate the adequate response of the DR 3 – TOU program in the developed scenario.

7.6. Complete Scenario

In this experiment, all the components described in section 8 are included. The experiment shows the interaction between the PV generator, battery system, loads, and grid coordinated by the EMS. Figure 44 shows the graphical results of the complete scenario simulation. Top trend of the figure shows the load power consumption using DR programs (red line), load power consumption without using DR programs (blue line), and SOC of the battery (aqua line). Middle trend of the figure shows the PV power generation (green line), utility grid power (orange line), and battery power (fuchsia line). The bottom trend shows the DR1 – TOU command (pink line), the DR2 – Shedding Low Level command (yellow line), and DR3 – Shedding Moderate Level command (purple line).

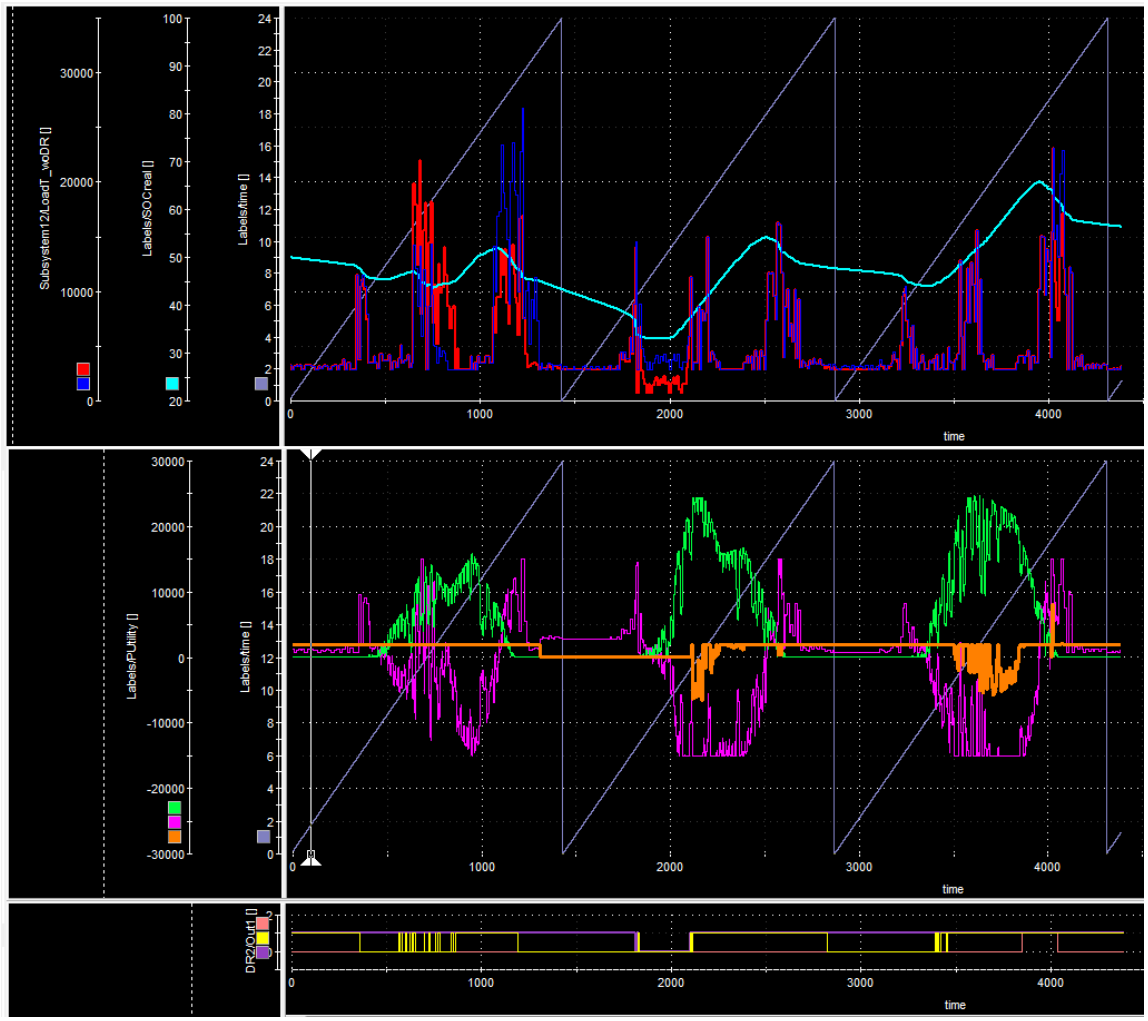

Figure 44. Complete scenario simulation

The objective of the EMS is to maximize the PV generation and to maintain a constant flow from the electrical grid, preserving the stability of the grid keeping a flat power demand. In this experiment, the objective grid power demand is 2 kW. EMS sets a power reference to the storage system depending of the power needed in the grid to supply the loads.

The experiment was configured to execute three days. The first day as a cloudy day, second as partially sunny, and last day as mostly sunny day. The experiment begins with the battery SOC in 50%, then the medium SOC level causes the DR1 command activation since the beginning.

At the beginning the grid and the battery support the needed power to supply a load with a demand around 3 kW. When the sun rises the battery begins to charge, but near to minute 650 the battery had to contribute to supply the loads because of the several clouds in the day. These power peaks are caused because DR1 command reschedule the activation of the washing and drying machine from the night to the day. It can be reflected in the different behaviors of the power load trends (with and without DR) during the day and night. The battery supplies the power peaks demanded during the first day in the morning and the night, generating a decrease of the SOC to a medium low level. It activates the DR2, then the external lights shedding during the night.

A blackout is simulated since minute 1310. It causes that the load power demand had to be supplied by the battery from here including the demand peak in the morning of the second day, having the effect of a fast decrease of SOC. This event takes the battery SOC to a low level, then the activation of DR3 in the minute 1820. This action helps the system to optimize the available energy and give time to improve the operation and a better energy generation. This energy optimization can be validated with the low decreasing behavior of the battery SOC and the DR command effects (comparing load trends with and without DR) between minute 1820 and 2115.

The grid recovers from the blackout at minute 2115. Due to the mostly sunny day, the PV generation levels are enough to charge the battery, supply the loads and inject power to the grid. Battery SOC recovers from the low level and reaches a medium level. Battery

covers the power peaks of the second day night and the third day morning with the grid in 2 kW. This battery use causes the DR2 activation, then the external lights shedding during the night.

The third day had a high power PV production, reaching a medium high SOC level and injecting a lot of power to the grid. Due to the medium high SOC level, the DR1 was disabled, then the washing and drying machine was able to be used in the night of the third day, generating high power peaks around minute 4021. Around this event, the PV power generation and the battery maximum power were not enough to supply the load demand. The grid power is flat in 2kW almost all the experiment, but these high power peaks causes that the grid had to supply this lack of power. The average grid power delivered in the experiment was 1.98 kW.

Table 14 shows the experiment numeric results. This results support the graphical analysis, confirming that the day 3 was the day with the most PV production with 151.47 kWh and also contributing to be the day with higher net metering with 41.82 kWh. The battery delivers more energy in day 2 (64 kWh) due to the blackout. Day 1 did not have power injected to the grid due to the poor PV generation.

Table 14. Complete scenario simulation numeric results

	Day 1	Day 2	Day 3
Photovoltaic System [kWh]	91.31	115.85	151.47
Battery System - Generated [kWh]	51.89	64.00	51.14
Battery System - Consumed [kWh]	(46.49)	(100.87)	(115.03)
Grid - Delivered [kWh]	44.06	23.42	41.82
Grid - Net Metering [kWh]	0.00	(4.27)	(9.63)
Residential Loads - Demanded [kWh]	(140.78)	(98.40)	(119.41)
Residential Loads w/o DR [kWh]	(141.25)	(106.12)	(121.52)

The load consumption analysis shows that the day with the most energy savings generated by DR was the second day. This is because of the activation of the DR2 early in the morning and in the night, also because of the load shedding with DR3 due to the low SOC level.

Chapter 8

CONCLUSIONS AND FUTURE WORK

8.1 Conclusions

The design and implementation of the HIL system, focusing in energy management system (EMS) and advance metering components, are described. The described modular structure of the setup allows an important level of flexibility. The flexibility of the platform allows to develop HIL scenarios with software modeled components or using both type, simulated and hardware in test components. These two features convert the setup in a powerful tool to construct a variety of applications and experiment scenarios with different sizes and complexity, related to microgrids, advance metering, renewable energy, and advance control.

Results show an EMS that that maximize the PV generation and effectively manage the Microgrid power flow. EMS also executes DR commands when the Microgrid needs energy savings and reduce power consumption with the objective to operate in the conditions descripted. A significant operation improvement in power consumption is achieved when DR take actions over the controlled loads avoiding an entire blackout in the Microgrid.

Experimental results demonstrate adequate response of the components on the scenario. The presented result in the work is a scenario with open research possibilities as advance power control, batteries modeling and characterization, photovoltaic panels modeling, components technology evaluation, and renewable system designs validation.

8.2 Contributions

The main contributions generated based on the thesis work are:

8.2.1. A novel Hardware-in-the-Loop microgrid platform conceptual design developed by the author is presented and documented in this work.

8.2.2. A running base scenario with open research possibilities is presented and documented. The Sustainable Energy Center (SEC) research team was trained to use this scenario to their investigations.

8.2.3. The content presented in this document served as the base information to generate two conference papers and one poster.

a. Paper "Advanced Metering Applications in Microgrids: A Hardware-in-the-Loop Electric Power Setup" accepted and presented in MEDPOWER 2018 – Dubrovnik, Croatia conference organized by IEEE.

b. Paper "An AC Microgrid Testbed for Power Electronics Courses in the University of Puerto Rico at Mayagüez" accepted and presented in IEEE ANDESCON – Cali, Colombia 2018 conference.

c. Poster "Hardware in the Loop (HIL) Simulation of a Photovoltaic Generator using a Texas Instrument Platform" accepted and presented in DistribuTECH 2017 – San Diego, California conference.

8.2.4. Other publication efforts:

a. Paper "Energy Management System for a Residential Microgrid in a Power Hardware-in-the-Loop Platform" submitted in IEEE PES 2019 General Meeting.

b. Paper "An AC Microgrid Testbed for Advance Metering Applications" accepted but not presented in CITREI 2018 – La Havana, Cuba conference.

8.3 Future Work

- Implementation of energy markets based on the microgrid scenario developed.
- Integration of the platform with other platforms or devices.
- Integration of third party smart meters to the HIL device by communication with the objective to integrate Advance Metering Infrastructure (AMI) projects to the laboratory.

- Development of complementary scenarios with more distributed components and additional features. Development of additional solar panel models, wind turbine models, storage systems models, complex grid models.
- Research in various microgrid control levels as voltage and current loops, droop control, synchronization control, connection and disconnection.

Bibliography

[1] A. Irizarry, E. O'Neill, and J. Colucci, "Achievable Renewable Energy Targets for Puerto Rico's Energy Portfolio Standard," 2009.

[2] L. Núm, "Ley Núm. 133 del año 2016," vol. 2016, no. 20, 2016.

[3] Puerto Rico Electric Power Authority, "Distribución porcentual de la generación de energía por tipo," *Official Website*, 2016. [Online]. Available: http://energia.pr.gov/datos/distribucion-porcentual-de-la-generacion-de-energia-por-tipo/.

[4] J. F. Patarroyo-Montenegro, J. E. Salazar-Duque, S. I. Alzate-Drada, J. D. Vasquez-Plaza, and F. Andrade, "An AC Microgrid Testbed for Power Electronics Courses in the University of Puerto Rico at Mayagüez," in *IEEE Andean Conference ANDESCON 2018*, 2018.

[5] S. Alzate-Drada, K. Montano-Martinez, F. Andrade, and A. Irizarry-Rivera, "Advanced Metering Applications in Microgrids: A Hardware-in-the-Loop Electric Power Setup," in *Mediterranean Conference on Power Generation, Transmission, Distribution and Energy Conversion MEDPOWER 2018*, 2018.

[6] R. M. Kennel, T. Boller, and J. Holtz, "Replacement of Electrical (Load) Drives by a Hardware-in-the-Loop System," in *International Aegean Conference on Electrical Machines and Power Electronics and Electromotion, Joint Conference*, 2011, pp. 17–25.

[7] B. Lu, X. Wu, H. Figueroa, and A. Monti, "A Low-Cost Real-Time Hardware-in-the-Loop Testing Approach of Power Electronics Controls," *IEEE Trans. Ind. Electron.*, vol. 54, no. 2, pp. 919–931, 2007.

[8] E. De Jong *et al.*, "European White Book on Real-Time Power Hardware-in-the-Loop Testing," 2011.

[9] O. Vodyakho, M. Steurer, C. S. Edrington, and F. Fleming, "An Induction Machine Emulator for High-Power Applications Utilizing Advanced Simulation Tools With

Graphical User Interfaces," *IEEE Trans. Energy Convers.*, vol. 27, no. 1, pp. 160–172, 2012.

[10] Z. Zhang and L. Fickert, "Power Hardware-in-the-Loop test of the energy feedback device in urban rail transportation system," in *2018 19th International Scientific Conference on Electric Power Engineering (EPE)*, 2018, pp. 1–4.

[11] Deparment of Energy, "Grid Modernization and the Smart Grid." [Online]. Available: https://www.energy.gov/oe/activities/technology-development/grid-modernization-and-smart-grid.

[12] National Institute of Standards and Technology, "NIST Special Publication 1108r3 NIST Framework and Roadmap for Smart Grid Interoperability NIST Special Publication 1108r3 NIST Framework and Roadmap for Smart Grid Interoperability," 2014.

[13] S. N. Kulkarni, "A review on Smart Grid Architecture and Implementation Challenges," pp. 3285–3290, 2016.

[14] H. Bentarzi and M. Tsebia, "PMU Based SCADA Enhancement in Smart Power Grid," in *2018 IEEE 12th International Conference on Compatibility, Power Electronics and Power Engineering (CPE-POWERENG 2018)*, 2018, pp. 1–6.

[15] P. B. Borase, "Energy Management System For Microgrid With Power Quality Improvement," in *2017 International conference on Microelectronic Devices, Circuits and Systems (ICMDCS)*, 2017, pp. 1–6.

[16] G. Latisko, D. Bhati, and V. Landenberger, "Application of IEC61970 and IEC61968 at KCP & L Smart Grid Demonstration Project," in *ISGT 2014*, 2014, pp. 1–5.

[17] Y. Ding, S. Member, C. Decker, I. Vassileva, and S. Member, "A Smart Energy System : Distributed Resource," in *2011 2nd IEEE PES International Conference and Exhibition on Innovative Smart Grid Technologies*, 2011, pp. 1–8.

[18] S. Sen and V. Agarwal, "Advanced Metering Infrastructure Analytics - A Case Study," in *2014 Eighteenth National Power Systems Conference (NPSC)*, 2014, pp. 1–6.

[19] S. Roy and B. Bedanta, "Advanced Metering Infrastructure for Real Time Load

Management in a Smart Grid," in *2015 International Conference on Power and Advanced Control Engineering (ICPACE)*, 2015, pp. 104–108.

[20] V. Narayan, A. Martínez, M. G. Jorge J., and G. Becerril, "Arteche Algorithms and their application in the estimation of states in smart grid," in *IEEE PES T&D 2010*, 2010, pp. 1–6.

[21] L. Li, S. W. Su, and W. Xiang, "Consensus-Based Smart Grid State Estimation Algorithm," *IEEE Trans. Ind. Informatics*, vol. 14, no. 8, pp. 3368–3375, 2018.

[22] G. P. System, Y. Li, X. Ren, and J. Niu, "Application of Rough Sets Theory in Forecast of Power Generation for," in *The 27th Chinese Control and Decision Conference (2015 CCDC)*, 2015, pp. 5064–5069.

[23] N. D. Hatziargyriou, A. G. Anastasiadis, J. Vasiljevska, and A. G. Tsikalakis, "Quantification of economic, environmental and operational benefits of microgrids," *2009 IEEE Bucharest PowerTech Innov. Ideas Towar. Electr. Grid Futur.*, pp. 1–8, 2009.

[24] Kema Inc., "Microgrids – Benefits, Models, Barriers and Suggested Policy Initiatives for the Commonwealth of Massachusetts," p. 66, 2014.

[25] S. L. H. Du, D. Z. W. Zhao, and M. G. Yao, "A Microgrid Energy Management System with Demand Response," in *2014 China International Conference on Electricity Distribution (CICED)*, 2014, pp. 23–26.

[26] J. M. Guerrero, S. Member, J. C. Vasquez, J. Matas, L. G. De Vicuña, and M. Castilla, "Hierarchical Control of Droop-Controlled AC and DC Microgrids — A General Approach Toward Standardization," vol. 58, no. 1, pp. 158–172, 2011.

[27] FERC, "Reports on Demand Response & Advanced Metering," 2017. [Online]. Available: https://www.ferc.gov/industries/electric/indus-act/demand-response/dem-res-adv-metering.asp.

[28] J. Zheng, D. W. Gao, and L. Lin, "Smart meters in smart grid: An overview," *IEEE Green Technol. Conf.*, pp. 57–64, 2013.

[29] Z. Popovic and V. Cackovic, "Advanced Metering Infrastructure in the context of Smart Grids," in *Energycon 2014*, 2014, pp. 1509–1514.

[30] J. Stromback, “Information Technologies in the House of the Future.”

[31] P. Palensky and D. Dietrich, “Demand side management: Demand response, intelligent energy systems, and smart loads,” *IEEE Trans. Ind. Informatics*, vol. 7, no. 3, pp. 381–388, 2011.

[32] P. Siano, “Demand response and smart grids — A survey,” *Renew. Sustain. Energy Rev.*, vol. 30, pp. 461–478, 2014.

[33] L. I. Minchala-Avila, J. Armijos, D. Pesántez, and Y. Zhang, “Design and Implementation of a Smart Meter with Demand Response Capabilities,” *Energy Procedia*, vol. 103, no. April, pp. 195–200, 2016.

[34] M. G. Vayá, M. Koller, S. Poelzig, M. Baldinger, and T. Borsche, “Demand Response based on smart metering Infrastructure to facilitate PV integration in low voltage grids,” in *CIRED Workshop 2016*, 2016, no. 0379, pp. 1–4.

[35] H. Kanchev, D. Lu, F. Colas, V. Lazarov, B. Francois, and S. Member, “Energy Management and Operational Planning of a Microgrid With a PV-Based Active Generator for Smart Grid Applications,” *IEEE Trans. Ind. Electron.*, vol. 58, no. 10, pp. 4583–4592, 2011.

[36] M. Stanovich, M. Sloderbeck, K. Schoder, J. Langston, I. Leonard, and S. Chatterjee, “Microgrid Control Using Remote Controller Hardware-in-the-Loop Over the Internet,” in *2018 IEEE Power & Energy Society Innovative Smart Grid Technologies Conference (ISGT)*, 2018, pp. 1–5.

[37] G. Walker, “Evaluating MPPT converter topologies using a Matlab PV Model,” *J. Electr. Electron. Eng. Aust.*, vol. 21, 2001.

[38] C. Roncero-Clemente, E. González-Romera, E. Romero-Cadaval, M. I. Milanés-Montero, and V. Miñambres-Marcos, “PSCAD / EMTDC Model for Photovoltaic Modules with MPPT based on Manufacturer Specifications,” in *Compatibility and Power Electronics (CPE), 2013 8th International Conference on, Ljubljana*, 2013, pp. 69–74.

[39] P. Sørensen and J. Fortmann, “Modular structure of wind turbine models in IEC 61400-27-1,” in *2013 IEEE Power & Energy Society General Meeting*, 2013, pp. 1–

5.

[40] C. Wang, Z. Fu, W. Huang, Y. Liu, and S. Zhang, “Doubly-fed Wind Turbine Mathematical Model and Simulation,” in *2014 International Symposium on Computer, Consumer and Control*, 2014, pp. 793–795.

[41] J. E. Carrasco and D. Serrano-jim, “A Ni-Cd battery model considering state of charge and hysteresis effects,” *J. Power Sources*, vol. 275, pp. 595–604, 2015.

[42] S. X. Chen, K. J. Tseng, and S. S. Choi, “Modeling of Lithium-Ion Battery for Energy Storage System Simulation,” in *2009 Asia-Pacific Power and Energy Engineering Conference*, 2009, pp. 1–4.

[43] A. Emadi and S. M. Ieee, “Modeling and Simulation of Electric and Hybrid Vehicles,” *Proc. IEEE*, vol. 95, no. 4, pp. 729–745, 2007.

[44] X. Meng, K. Lin, A. Model, and P. Cell, “Research on photovoltaic power system of microgrid based on real-time simulation,” in *2017 IEEE Conference on Energy Internet and Energy System Integration (EI2)*, 2017, pp. 1–5.

[45] T. Yun, Y. Dong, Y. Libin, and H. Qian, “Research and Realization of Hardware - in - the - loop Simulation Technology for Photovoltaic Power Generation System Based on ADPSS,” in *2017 10th International Conference on Intelligent Computation Technology and Automation (ICICTA)*, 2017, pp. 54–57.

[46] J. Li, B. Zhou, and H. Guo, “Hardware-In-Loop Simulation of Wind Turbine Based on BLDCM,” in *2009 World Non-Grid-Connected Wind Power and Energy Conference*, 2009, pp. 1–5.

[47] J. Chen and D. Jiang, “Study on Modeling and Simulation of Non-grid- connected Wind Turbine,” in *2009 World Non-Grid-Connected Wind Power and Energy Conference*, 2009, no. 2, pp. 1–5.

[48] M. Y. W. Teow, H. K. Chiu, and R. H. G. Tan, “A computational modelling of wind turbine mechanical power and its improve factor determination,” in *4th IET Clean Energy and Technology Conference (CEAT 2016)*, 2016, pp. 1–8.

[49] A. Alsharkawi and J. A. Rossiter, “Modelling Analysis of a Solar Thermal Power Plant,” in *2017 6th International Conference on Clean Electrical Power (ICCEP)*,

2017, pp. 694–698.

[50] S. Mirela, Ț Tucb, and D. Toma, “Mathematical modeling and simulation of a thermal system using solar radiation as energy source,” in *2017 International Conference on ENERGY and ENVIRONMENT (CIEM)*, 2017, no. 7, pp. 368–371.

[51] G. Lixin, “Numerical Simulation of the Thermal Performance of Solarwall,” in *2011 Third International Conference on Measuring Technology and Mechatronics Automation*, 2011, vol. 2, no. 1, pp. 721–724.

[52] A. G. Yepes and F. D. Freijedo, “High-Performance Digital Resonant Controllers Implemented With Two Integrators,” *IEEE Trans. Power Electron.*, vol. 26, no. 2, pp. 563–576, 2011.

[53] M. Parchomiuk, “Modular Power Converter with Superconducting Magnetic Energy Storage for Electric Power Distribution System – Analysis and Simulation,” in *2017 19th European Conference on Power Electronics and Applications (EPE’17 ECCE Europe)*, 2017, pp. 1–6.

[54] M. Parchomiuk, R. Strzelecki, K. Zymmer, and A. Domino, “Modular Power Converter Topologies for Energy Storage and Electric Power Distribution Systems,” in *2017 Progress in Applied Electrical Engineering (PAEE)*, 2017, pp. 1–6.

[55] M. Bounabi, M. S. Ait-cheikh, and Z. Dahmane, “Hardware-in-the-Loop FPGA-based Real-time simulation of Cascaded H-Bridge Multilevel Inverter for Grid Interactive Photovoltaic Power Plant,” in *2017 IEEE Manchester PowerTech*, 2017, pp. 7–11.

[56] T. Xia, M. Li, P. Zi, L. Tian, X. Qin, and N. An, “Modeling and Simulation of Battery Energy Storage System (BESS) Used in Power System,” *2015 5th Int. Conf. Electr. Util. Deregul. Restruct. Power Technol.*, pp. 2120–2125, 2015.

[57] R. Mo, M. Steurer, and H. Li, “Controller Hardware-in-the-loop (CHIL) Simulation of a Multi-functional Energy Storage System Based on Modular Multilevel DC / DC Converter (M2DC) for MVDC Grid,” *2016 IEEE 8th Int. Power Electron. Motion Control Conf. (IPEMC-ECCE Asia)*, pp. 1980–1984, 2016.

[58] K. S. Kavithakumari, “Advance Metering Infrastructure for Smart Grid using GSM,” in *2017 Third International Conference on Science Technology Engineering &*

Management (ICONSTEM), 2017, pp. 619–622.

[59] I. Petruševski, G. S. Member, M. Živanović, and A. Rakić, "Novel AMI Architecture for Real-Time Smart Metering," in *2014 22nd Telecommunications Forum Telfor (TELFOR)*, 2014, pp. 664–667.

[60] G. Wibisono, G. P. S, E. Eng, and U. Indonesia, "Development of Advanced Metering Infrastructure Based on LoRa WAN in PLN Bali Toward Bali Eco Smart Grid," in *2017 Saudi Arabia Smart Grid (SASG)*, 2016, pp. 4–7.

[61] M. Carratù, M. Ferro, and A. Pietrosanto, "Smart Power Meter for the IoT," in *2018 IEEE 16th International Conference on Industrial Informatics (INDIN)*, 2018, pp. 514–519.

[62] N. A. Kulatunga, I. Member, S. Navaratne, J. Dole, C. Liyanagedera, and T. Martin, "Hardware Development for Smart Meter Based Innovations," *IEEE PES Innov. Smart Grid Technol.*, pp. 1–5, 2012.

[63] A. Gaikwad and P. Markham, "Implementation of the WECC Composite Load Model for Utilities using the Component-Based Modeling Approach," *2016 IEEE/PES Transm. Distrib. Conf. Expo.*, pp. 1–5, 2016.

[64] S. Arora, P. T. Balsara, D. K. Bhatia, and A. C. P. Loads, "Digital Implementation of Constant Power Load (CPL), Active Resistive Load , Constant Current Load and Combinations," in *2016 IEEE Dallas Circuits and Systems Conference (DCAS)*, 2016, pp. 5–8.

[65] A. Gomes, M. Ieee, C. H. Antunes, and A. G. Martins, "Physically-Based Load Demand Models for Assessing Electric Load Control Actions," *2009 IEEE Bucharest PowerTech*, pp. 1–8, 2009.

[66] Y. Liu, M. Marz, T. Ortmeyer, and V. Rajagopalan, "Test systems for harmonics modeling and simulation," *IEEE Trans. Power Deliv.*, vol. 14, no. 2, pp. 579–587, 1999.

[67] T. S. Theodoro, P. G. Barbosa, M. A. Tomim, A. C. S. De Lima, and M. T. C. De Barros, "MatLab-OpenDSS Co-Simulation Environment : An Alternative Tool to Investigate DSG Connection," in *2018 Simposio Brasileiro de Sistemas Eletricos (SBSE)*, 2018,

pp. 1–7.

[68] W. H. Kersting, “The Simulation of Loop Flow in Radial Distribution Analysis Programs,” *IEEE Trans. Ind. Appl.*, vol. 51, no. 2, pp. 1928–1932, 2015.

[69] K. Balasubramaniam and S. Abhyankar, “A Combined Transmission and Distribution System Co-Simulation Framework for Assessing the Impact of Volt / VAR Control on Transmission System,” in *2017 IEEE Power & Energy Society General Meeting*, 2017, pp. 1–5.

[70] K. H. S. V. S. Nunna and S. Doolla, “Responsive end-user-based demand side management in multimicrogrid environment,” *IEEE Trans. Ind. Informatics*, vol. 10, no. 2, pp. 1262–1272, 2014.

Appendix A

$$I = I_L - I_O\left(e^{\frac{q(V+I*R_S)}{nkT}} - 1\right)$$

$$I_L = I_{L(T_1)}\left(1 + K_o(T - T_1)\right)$$

$$I_{L(T_1)} = G * \frac{I_{SC(T_1,nom)}}{G_{(nom)}}$$

$$K_o = \frac{I_{SC(T_2)} - I_{SC(T_1)}}{T_2 - T_1}$$

$$I_O = I_{O(T_1)} * \left(\frac{T}{T_1}\right)^{\frac{3}{n}} * e^{-\frac{qV_g}{nk\left(\frac{1}{T} - \frac{1}{T_1}\right)}}$$

$$I_{O(T_1)} = \frac{I_{SC(T_1)}}{e^{\frac{qV_{OC(T_1)}}{nkT_1}} - 1}$$

$Where$:

G: $irradiance$

T: $temperature$

k: $Boltzman's\ constant$

q: $charge\ on\ an\ electron$

R_s: $series\ resistance$

R_P: $shunt\ resistance\ in\ parallel\ with\ the\ diode$

n: $diode\ quality\ factor$

I_L: $photo\ generated\ current$

I_o: $diode\ saturation\ current$

K_o: $current\ variaton\ rate\ between\ T_1\ and\ T_2$

I_{SC}: $short\ circuit\ current$

V_{OC}: $open\ circuit\ voltage$

V_g: $band\ gap\ voltage$

V_m: $voltage, maximum\ power$

I_m: $current, maximum\ power$

P_m: $maximum\ power$

Appendix B

Rule Num.	SOC	Pbat	DR1	DR2	DR3
1	L	(-)H	**On**	**On**	**On**
2	L	(-)M	**On**	**On**	**On**
3	L	(-)L	**On**	**On**	**On**
4	L	(+)L	**On**	**On**	**On**
5	L	(+)M	**On**	**On**	**On**
6	L	(+)H	**On**	**On**	**On**
7	ML	(-)H	**On**	Off	Off
8	ML	(-)M	**On**	Off	Off
9	ML	(-)L	**On**	**On**	Off
10	ML	(+)L	**On**	**On**	Off
11	ML	(+)M	**On**	**On**	Off
12	ML	(+)H	**On**	**On**	Off
13	M	(-)H	**On**	Off	Off
14	M	(-)M	**On**	Off	Off
15	M	(-)L	**On**	Off	Off
16	M	(+)L	**On**	Off	Off
17	M	(+)M	**On**	Off	Off
18	M	(+)H	**On**	Off	Off
19	MH	(-)H	Off	Off	Off
20	MH	(-)M	Off	Off	Off
21	MH	(-)L	Off	Off	Off
22	MH	(+)L	Off	Off	Off
23	MH	(+)M	Off	Off	Off
24	MH	(+)H	Off	Off	Off
25	H	(-)H	Off	Off	Off
26	H	(-)M	Off	Off	Off
27	H	(-)L	Off	Off	Off
28	H	(+)L	Off	Off	Off
29	H	(+)M	Off	Off	Off
30	H	(+)H	Off	Off	Off